

Copyright
by
Andrew Christopher Popielski
2011

**The Thesis Committee for Andrew Christopher Popielski
Certifies that this is the approved version of the following thesis:**

**Rock Classification from Conventional Well Logs in Hydrocarbon-
Bearing Shale**

**APPROVED BY
SUPERVISING COMMITTEE:**

Supervisor:

Carlos Torres-Verdín

Matthew Balhoff

**Rock Classification from Conventional Well Logs in Hydrocarbon-
Bearing Shale**

by

Andrew Christopher Popielski, B.S.E.

Thesis

Presented to the Faculty of the Graduate School of

The University of Texas at Austin

in Partial Fulfillment

of the Requirements

for the Degree of

Master of Science in Engineering

The University of Texas at Austin

December 2011

Acknowledgements

I would like to thank Dr. Carlos Torres-Verdín for his patience and assistance with my work on this project. I would also like to thank him for teaching me the importance of attention to detail. Dr. Matthew Balhoff has my gratitude for agreeing to read this thesis.

I would like to acknowledge my mother–Gabriela Schell, my sister–Sophia Evans, and my brother-in-law–Josh Evans for their encouragement. Jim Keller and Augustine Mathews deserve special recognition for their support and obvious interest in the success of my pursuits.

It was a pleasure to work with all of my colleagues in the Formation Evaluation group, especially Philippe Marouby, Antoine Montaut, Zoya Heidari, Rohollah A. Pour, and Ben Voss.

I am grateful to ConocoPhillips and BP for allowing the publication of this data. Jesus M. Salazar from ConocoPhillips deserves special thanks for mentoring me during an internship in the Summer of 2010. Thaimar Ramirez was very helpful during the same internship and also of invaluable support in acquiring data at my request. I would like to acknowledge Edwin Ortega for getting nice thin-section and SEM images for me.

The work reported in this thesis was funded by the University of Texas at Austin’s Research Consortium on Formation Evaluation, jointly sponsored by Anadarko, Apache, Aramco, Baker Hughes, BG, BHP Billiton, BP, Chevron, ConocoPhillips, ENI, ExxonMobil, Halliburton, Hess, Maersk, Marathon Oil Corporation, Mexican Institute for Petroleum, Nexen, ONGC, Petrobras, Repsol, RWE, Schlumberger, Statoil, TOTAL, and Weatherford.

Abstract

Rock Classification from Conventional Well Logs in Hydrocarbon-Bearing Shale

Andrew Christopher Popielski, M.S.E.

The University of Texas at Austin, 2011

Supervisor: Carlos Torres-Verdín

This thesis introduces a rock typing method for application in shale gas reservoirs using conventional well logs and core data. Shale gas reservoirs are known to be highly heterogeneous and often require new or modified petrophysical techniques for accurate reservoir evaluation. In the past, petrophysical description of shale gas reservoirs with well logs has been focused to quantifying rock composition and organic-matter concentration. These solutions often require many assumptions and ad-hoc correlations where the interpretation becomes a core matching exercise. Scale effects on measurements are typically neglected in core matching. Rock typing in shale gas provides an alternative description by segmenting the reservoir into petrophysically-similar groups with k-means cluster analysis which can then be used for ranking and detailed analysis of depth zones favorable for production.

A synthetic example illustrates the rock typing method for an idealized sequence of beds penetrated by a vertical well. Results and analysis from the synthetic example show that rock types from inverted log properties correctly identify the most organic-rich

model types better than rock types detected from well logs in thin beds. Also, estimated kerogen concentration is shown to be most reliable in an under-determined problem.

Field cases in the Barnett and Haynesville shale gas plays show the importance of core data for supplementing well logs and identifying correlations for desirable reservoir properties (kerogen/TOC concentration, gas saturation, and porosity). Qualitative rock classes are formed and verified using inverted estimates of kerogen concentration as a rock-quality metric. Inverted log properties identify 40% more of a high-kerogen rock type over well-log based rock types in the Barnett formation. A case in the Haynesville formation suggests the possibility of identifying depositional environments as a result of rock attributes that produce distinct groupings from k-means cluster analysis with well logs. Core data and inversion results indicate homogeneity in the Haynesville formation case. However, the distributions of rock types show a 50% occurrence between two rock types over 90 ft vertical-extent of reservoir. Rock types suggest vertical distributions that exhibit similar rock attributes with characteristic properties (porosity, organic concentration and maturity, and gas saturation).

This method does not directly quantify reservoir parameters and would not serve the purpose of quantifying gas-in-place. Rock typing in shale gas with conventional well logs forms qualitative rock classes which can be used to calculate net-to-gross, validate conventional interpretation methods, perform well-to-well correlations, and establish facies distributions for integrated reservoir modeling in hydrocarbon-bearing shale.

Table of Contents

List of Tables	ix
List of Figures	x
Chapter 1: Introduction	1
1.1 Background	1
1.2 Objectives	2
1.3 Outline.....	5
Chapter 2: Methods	6
2.1 Well-Log and Core Alignment	7
2.2 Model Development and Inversion.....	8
2.2.1 Bed-Boundary Selection	8
2.2.2 Mineral Model Development.....	9
2.2.3 Inversion Results.....	10
2.3 Core Relationships and Log-based Rock Typing	10
2.4 Rock Typing.....	11
2.5 Rock Typing Validation with Rock Compositional Results from Inversion	12
Chapter 3: Synthetic Case	13
3.1 Development and Results of the Synthetic Case	13
3.2 Applicability to Log-based Rock Typing in the Field	20
Chapter 4: Field Examples of Rock Typing	21
4.1 Field Example: Barnett Shale Gas Play	21
4.1.1 Geological and Geochemical Background.....	21
4.1.2 Log Response and Rock Property Relationship.....	22
4.1.3 Rock Typing in the Lower Barnett Formation.....	24
4.1.4 Significance of Resolution and Rock Typing	30
4.2 Field Example in the Haynesville Formation	33
4.2.1 Geological Background	33

4.2.2 Well Log Response and Rock-Property Relationships	33
Chapter 5: Discussion	41
5.1 Discussion on the Importance of Mechanical Properties and Fractures	41
5.2 Discussion on the Importance of Kerogen Maturity and Core Data.....	45
Chapter 6: Conclusions	46
6.1 Conclusions.....	46
6.2 Suggestions for Future Work	48
Appendix A: Nonlinear Joint Inversion of Well Logs	49
A.1 Model Development.....	49
A.1.1 Bed-Boundary Selection	49
A.1.2 Mineral Model.....	50
A.2 Inversion Method	50
A.3 Application of Nonlinear Inversion to The Barnett formation Field Example	52
Appendix B: Calculation of TOC based on Passey's Method	59
Glossary	62
References.....	64

List of Tables

Table 3.1:	Hypothetical solid and fluid constituents for three rock types included in the shale gas synthetic model. Volumetric concentrations of all lithological components plus porosity sum to 100 %. Water and methane saturations are displayed as a percentage of pore space concentration.	14
Table 3.2:	Average error between model mineralogy and inverted mineralogy for even- and under-determined problems.	19
Table 3.3:	Advantages and disadvantages of rock typing when using different levels of data refinement.	20
Table 4.1:	Proposed rock types based on the cluster analysis of well logs and validated with multi-mineral inversion results. Thin section images and corresponding compositions are included for the proposed rock types.	27
Table 4.2:	Standard deviations of well logs used in the cluster analysis and pertinent core data (TOC, porosity, water saturation, and bulk density).	35
Table 4.3:	Proposed rock types based on cluster analysis of well logs and inverted kerogen concentration.	40
Table A.1:	Mineral, fluid, and resistivity values assumed in rock-compositional inversion for the lower Barnett formation well.	58

List of Figures

Figure 1.1: Microscopic views of kerogen-rich rock: (a) thin section at 0.5 mm and (b) backscattered SEM at 30 μm . Kerogen appears black in (b).	4
Figure 2.1: Flow chart summarizing the procedures advanced in this thesis to perform rock typing from well logs.	7
Figure 2.2: Well logs underlain with the corresponding electrical image log (FMI) and hypothetical bed boundaries (dashed green lines). Logs are arranged in order of highest to lowest vertical resolution from left to right. Track 1: Depth. Track 2: Resistivity and formation image. Track 3: Gamma ray and formation image. Track 4: Neutron porosity (in limestone units) and formation image. Track 5: Bulk density and formation image.	9
Figure 3.1: Synthetic model: average error between inverted and model properties over individual sections of 0.5, 1, 2, and 10 ft bed thicknesses. Tool resolution and sampling rate cause the error to increase with decreasing bed thickness.	15
Figure 3.2: Synthetic case showing the progression from thick beds to thin beds and the associated well logs. Track 1: Bed thicknesses for the corresponding interval in a progression from 10 ft beds to 0.5 ft beds. Tracks 2–5: Simulated, model, inverted, and center-bed values for neutron porosity (limestone units), bulk density, PEF, and resistivity, respectively. Tracks 6–9: Cluster analysis results for actual rock types obtained from inverted properties, center-bed values, and log values.	17

Figure 3.3: Synthetic case: multi-mineral inversion rock typing with model rock types, an even-determined solution, and an under-determined solution. Track 1: Bed thicknesses within the interval. Track 2: Model composition. Track 3: Model rock types. Track 4: Rock-compositional estimates for an even-determined solution. Track 5: Rock types determined from k-means cluster analysis based upon estimated mineral compositions in Track 4. Track 6: Rock-compositional estimates from an under-determined solution. Track 7: Rock types determined from k-means cluster analysis based upon estimated mineral compositions shown in Track 6.....	18
Figure 4.1: The three-dimensional cross-plot shows the relationship between core-measured kerogen (volumetric percent), porosity (volumetric percent), and water saturation (S_w , percent of pore space); the color scale indicates the corresponding core-measured bulk density. The log track (right) shows a formation image overlain by the bulk density well log.	23
Figure 4.2: Biplot for factor analysis for the lower Barnett formation. Projections are labeled with the corresponding well logs. Colors designate statistically significant relationships between groups of well logs. The projection labeled 'Sonic' refers to compressional sonic slowness.	24
Figure 4.3: Cross-plots and histograms of cluster groupings: (a) well log measurements of resistivity, bulk density, and neutron porosity (in limestone units) and (b) inverted properties for resistivity, bulk density, and migration length (L_m).	26

Figure 4.4:	Inverted log properties, formation image, rock typing, and mineralogy. Track 1: Relative depth. Track 2: Apparent resistivity and inverted resistivity. Track 3: Neutron porosity (in limestone units) and inverted migration length. Track 4: PEF and inverted PEF. Track 5: Bulk density and inverted density. Track 6: Electrical image. Track 7: Log-based rock types. Track 8: Rock types from inverted properties.....	29
Figure 4.5:	Average volumetric concentration of kerogen for different rock types; kerogen concentration is estimated with nonlinear inversion.....	30
Figure 4.6:	Thin beds and comparison of kerogen volumetric concentration estimated from inversion and conventional methods. Track 1: Relative depth. Track 2: Comparison of TOC derived with Passey's method (Passey et al., 1990), nonlinear inversion, and laboratory core. Track 3: Log-based rock types. Track 4: Inverted-property-based rock types. Track 5: Mineralogy estimated with nonlinear inversion. Track 6: Mineralogy estimated with a commercial linear solver.....	32
Figure 4.7:	Three-dimensional cross-plot showing the relationship between core-measured TOC (weight percent), porosity (volumetric percent), and water saturation (S_w , percent of pore space); the color scale identifies the corresponding core-measured bulk density. The blue oval designates the core points within the studied depth-interval.....	34
Figure 4.8:	Factor analysis for the depth interval within the Haynesville shale gas play. Colors designate statistically significant relationships between logs.....	36

Figure 4.9: Cross-plots and histograms of cluster groupings: (a) well logs for apparent deep resistivity, bulk density, and neutron porosity (in limestone units) and (b) inverted properties for resistivity, bulk density, and migration length (Lm).	37
Figure 4.10: Inverted log properties and well logs, core data, rock typing, and mineralogy. Track 1: Relative depth. Track 2: Neutron porosity (in limestone units) and inverted migration length. Track 3: Bulk density and inverted bulk density. Track 4: Apparent deep resistivity and inverted resistivity. Track 5: Core TOC. Track 6: Core porosity. Track 7: Core saturation. Track 8: Rock types from well logs. Track 9: Rock types from inverted log properties. Track 10: Rock-composition estimates obtained from nonlinear inversion	39
Figure 5.1: Rose diagram showing the high concentration of natural and drilling-induced fractures in the lower Barnett formation study interval (90 ft). The azimuth of drilling-induced fractures indicates the maximum horizontal stress.	42
Figure 5.2: A core-slab photo (left) shows mineralized, high-angle, natural fractures. At right: Track 1 shows the electrical formation image; Track 2 shows the separation of array induction resistivity logs. The formation image displays dark (electrically conductive) sinusoidal features which are interpreted to belong to the same natural fracture type as those observed in the core-slab photo.	44
Figure A.1: Generalized mineral model assumed for volumetric calculations in Haynesville formation and Barnett formation shale gas plays.	50

Figure A.2: Adjustment of resistivity exponents (a , m , n) by matching core saturation, porosity, and estimated connate-water resistivity to available resistivity measurements. For Class 1: $a=1$, $m=2.05$, $n=2$; for Class 2: $a=1$, $m=2.3$, $n=2$; for Class 3: $a=1$, $m=2.1$, $n=2$; for Class 4: $a=1$, $m=1.7$, $n=1.5$.	54
Figure A.3: Inverted layer properties compared to field measurements. Track 1: Measured and inverted density. Track 2: Measured and inverted PEF. Track 3: Measured and inverted migration length. Track 4: Measured and inverted deep resistivity.	55
Figure A.4: Estimated shale composition from nonlinear inversion. Track 1: Total porosity. Track 2: Water saturation. Track 3: Volumetric concentration of kerogen. Track 4: Volumetric concentration of quartz. Track 5: Volumetric concentration of calcite. Track 6: Volumetric concentration of pyrite. Track 7: Volumetric concentration of clay.	56
Figure A.5: Well logs numerically simulated from estimated rock components and their agreement with well logs. Track 1: Measured and simulated PEF. Track 2: Measured and simulated bulk density. Track 3: Measured and simulated neutron porosity (in limestone units). Track 4: Measured and simulated apparent deep resistivity.	57
Figure B.1: Determination of LOM from a cross-plot of S2 vs. TOC obtained from laboratory measurements.	60

Figure B.2: Display of inputs and results from Passey's TOC-calculation method (Passey et al., 1990). Track 1: Relative depth. Track 2: Resistivity and density logs with grey shading indicating separation between the logs. Track 3: Delta log R calculated from the separation between density and resistivity. Track 4: TOC from Passey's method compared to core data. Track 5: Comparison between sonic/resistivity TOC calculation and density/resistivity TOC calculation.....61

Chapter 1: Introduction

The composition of shale gas reservoirs is known to be highly heterogeneous in the vertical direction as a result of variable and complex rock components. These reservoirs exist as self-contained petroleum systems, serving as the source, seal, and reservoir for natural gas. Petrophysical analyses are complicated by the finely dispersed assortment of unique solid and fluid constituents that result from the sourcing organic matter, cracked oil and gas, and low energy depositional environments. Permeability is extremely low in shale gas formations and the economic production of hydrocarbon is possible in large part by the advent of horizontal drilling and modern completions technologies. However, the identification of zones that are likely to provide the maximum output over the life of a well cannot be treated without due consideration. A comprehensive analysis of pilot-hole well logs is crucial to evaluate the potential of a well.

According to a study published by the National Petroleum Council, identifying shale facies using geochemical source analysis and well logs has been listed as a moderately significant technology anticipated to be developed by the year 2020. The outcome of accurate facies identification is intended to facilitate an increase in the exploration success rate in shale gas formations (Perry et al., 2007). This thesis focuses on facies identification, also known as rock typing or rock classification, in shale gas reservoirs. A successful application of rock typing can assist in determining net-to-gross (NTG) and contribute to reservoir description for application in integrated reservoir models.

1.1 BACKGROUND

The objective for any shale gas prospect is to effectively fracture and produce hydrocarbons from organic-rich strata (Chong et al., 2010). Rock types represent rocks in and around a potentially productive reservoir which are grouped based on a set of similar properties. These properties should identify attributes which correspond to reservoir quality. Previous rock typing methods in conventional reservoirs have been based on the grouping of rocks with similar storage and flow capacity. Storage and flow capacity were represented by permeability and

porosity, respectively (Winland and Pittman, 1992; Amaefule et al., 1993). Unconventional reservoirs require a different approach due to the aforementioned complexities. Kale et al. (2010) developed a rock typing method for shale gas based on core measurements over a wide range of reservoir rock in the Newark East field of the Barnett shale gas play (800 core plugs over 1600 ft of core from four wells). They measured porosity, total organic carbon (TOC), mineralogy, and mercury injection capillary pressure at discrete core points. These properties were used to assign rock types over the intervals of study, partly through statistical methods.

Hammes (2010) suggests that rock attributes such as mineralogy, organic matter abundance, organic matter type/maturity, and pore size are related to depositional environments. These depositional environments may be predictable from facies distribution models which can then be related to reservoir characteristics.

Petrophysical evaluation in shale gas relies on log-based multi-mineral estimation. Such interpretations generally require calibration and validation with core data (Quirein et al., 2010). Spears and Jackson (2009) describe the importance of accurate estimation of volumetric mineral concentrations, organic content, and porosity. They identify organic content, measured by TOC or kerogen concentration, as measures of gas-shale quality. Heidari et al. (2010, 2011) developed a deterministic nonlinear inversion method to estimate volumetric concentrations of rock components for applications in conventional reservoirs and shale gas reservoirs. This method was shown to produce reliable quantitative estimates of mineralogy, porosity, kerogen concentration, and saturation when compared to core data. Rock-composition quantities presented in this thesis are calculated with the code developed for shale gas applications by Heidari et al. (2011).

1.2 OBJECTIVES

Literature does not provide an instance, to the author's knowledge, of a log-based rock typing approach specifically applied to shale gas. The methods presented in this thesis are

closely tied to core, but attempt to extend core observations to the reservoir as a whole using well logs. The nonlinear multi-mineral inversion technique developed by Heidari et al. (2011) is assumed to be a valid method for the estimation of mineralogy from conventional well logs. Rock typing attempts to extend the concept of an earth model of layered beds with unique compositions and resultant physical properties. Figure 1.1a shows a microscopic thin-section of an organic-rich black shale layer overlying a calcite-rich layer. The demarcation between facies is clear and provides an example of separate rock types that exhibit layering. Figure 1.1b shows a backscattered SEM image of an organic-rich section that contains pyrite, dolomite, calcite, illite, mica, and kerogen. This picture provides evidence of dispersed kerogen and the compositionally variable matrix that must be explained in petrophysical analysis.

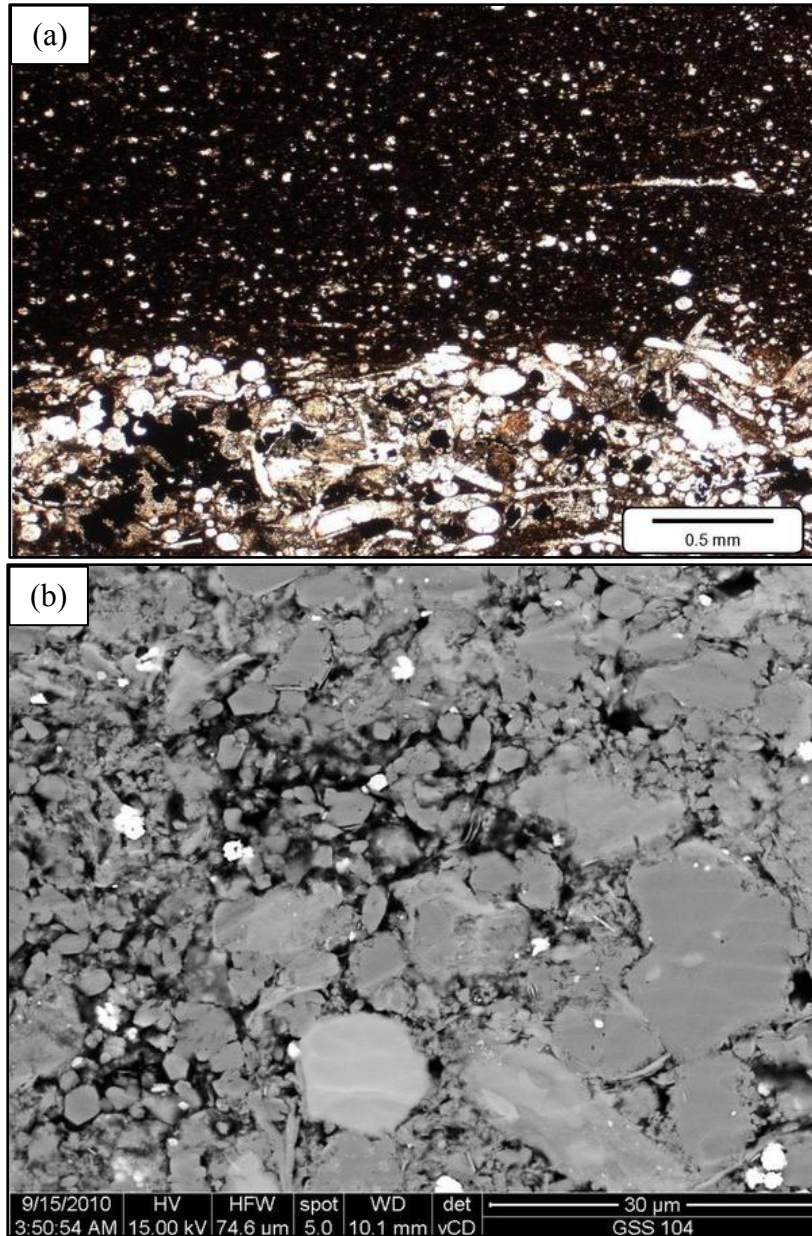


Figure 1.1: Microscopic views of kerogen-rich rock: (a) thin section at 0.5 mm and (b) backscattered SEM at 30 μm . Kerogen appears black in (b).

The rock typing method described in this thesis is founded upon existing trends in core data. Core data are used to identify correlations and provide a connection to the interpretation of well logs. Statistical techniques are utilized with well logs to expose associations between well logs. These statistical techniques are k-means cluster analysis and factor analysis. Such

techniques are useful to analyze large amounts of complex data which are typically available in shale gas exploratory wells.

1.3 OUTLINE

Chapter 2 of this thesis outlines the methods, assumptions, and approach considered for rock typing in shale gas formations. Chapter 3 describes a synthetic case to illustrate rock typing and its limitations with application to field logs, inverted bed properties, and mineralogy. Chapter 4 introduces field cases from the lower Barnett and Haynesville formations with an initial emphasis on core data; inferences are made to establish an association with well logs. Well logs and inverted properties are classified using k-means cluster analysis. Chapter 5 discusses the importance of fractures, mechanical properties, and kerogen maturity of hydrocarbon-bearing shales as they impact rock typing. The outcomes, potential applications, and recommendations for future work are presented in Chapter 6. Appendix A is dedicated to a concise description of concepts and application of the nonlinear inversion developed by Heidari et al. (2011). Appendix B is an overview of Passey et al.'s (1990) method for TOC estimation.

Chapter 2: Methods

Rock typing in shale gas is applied under the assumption that a combination of well logs can identify rock groups that exhibit similar compositional attributes. Statistical techniques are well-suited for the analysis of shale gas reservoirs since trends may be obscured by heterogeneity. When applied to conventional well logs, statistical techniques are impacted by shoulder-bed effects, differences in vertical resolution, and depth alignment. Data quality can be enriched with inversion techniques. The objective in this study is to ascertain whether: (a) well logs can be used to perform rock typing in shale gas, and (b) whether inversion of layer properties provides an advantage in rock typing by the minimization of shoulder-bed effects and vertical resolution refinement. The procedure to address the points above is performed by: (1) log and core alignment, (2) implementation of inversion to estimate layer properties (true resistivity (R_t), migration length (L_m), photoelectric factor (PEF), density) and subsequent estimates of rock compositions, (3) exploring relationships between core data and well logs and performing k-means cluster analysis for well-log-based rock typing, (4) validating the log-based rock types with rock-composition estimates obtained from inversion. Figure 2.1 is a flow chart of the procedures detailed below.

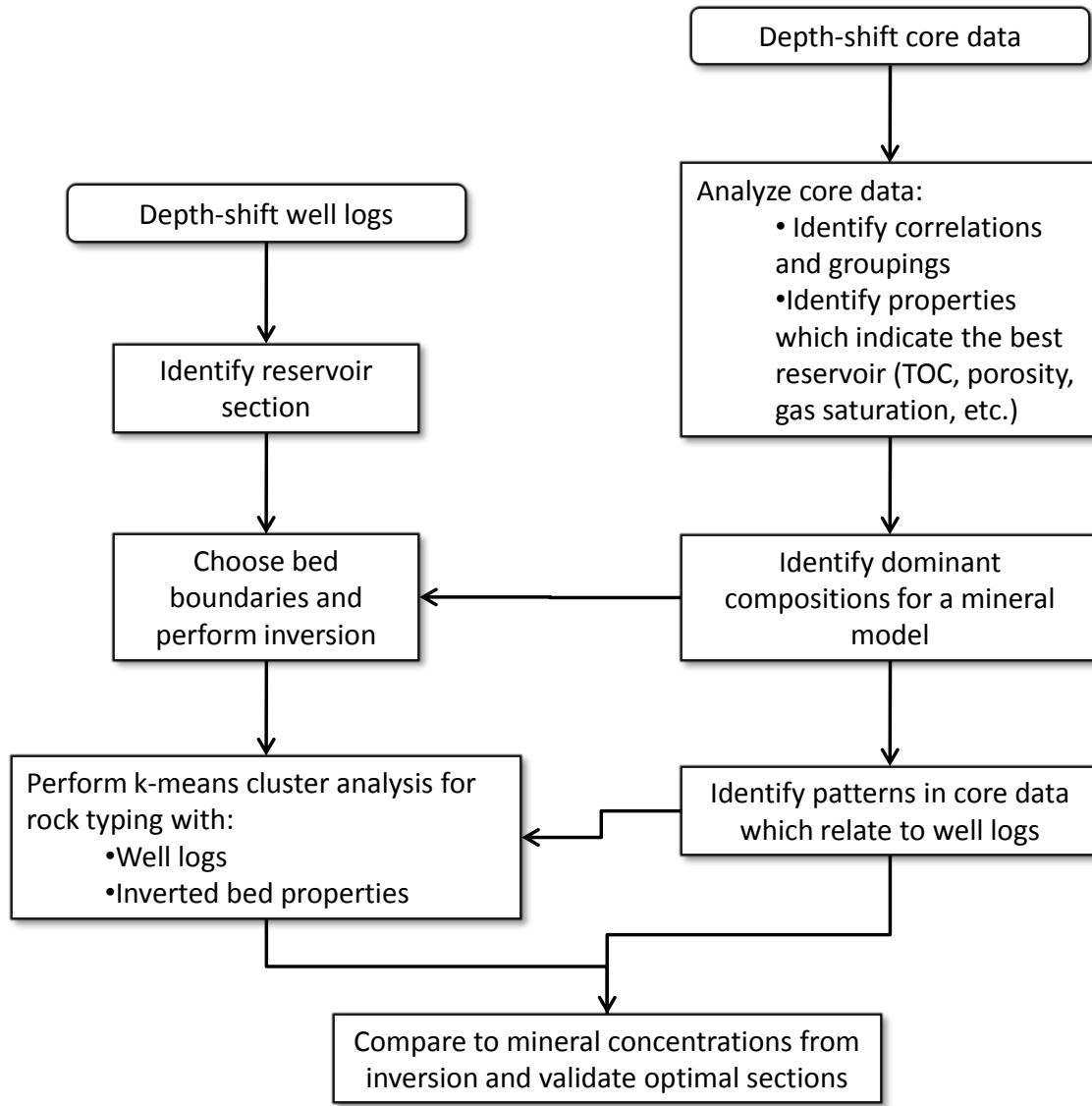


Figure 2.1: Flow chart summarizing the procedures advanced in this thesis to perform rock typing from well logs.

2.1 WELL-LOG AND CORE ALIGNMENT

Log and core alignment are prerequisites for well log analysis. Alignment corrections ensure that all downhole measurements are representative of the same point along the wellbore. Log responses tend to lose coherence with each other in cases of: (a) averaging due to thin beds, (b) caliper irregularities, (c) noise, and (d) filtering. Although automatic depth-alignment software is available, the best results are usually achieved with manual adjustment. In many

cases, optimal alignment cannot be detected; in this case the measurements were not altered to avoid creating physically misrepresentative logs. Core data are usually delivered from a laboratory in a depth-uncorrected state due to differing wireline and coring depth measurements. Wireline and core depth must be reconciled for calibration, comparison, and model development. Typically, a core gamma-ray log is generated from the whole-core section and then depth-matched to the wireline gamma-ray response.

2.2 MODEL DEVELOPMENT AND INVERSION

Inversion techniques provide estimates of formation properties that are crucial to the evaluation of shale gas reservoirs. Heidari et al. (2011) produced and successfully applied a two-step inversion technique that is utilized in this thesis. Layer properties estimated from the joint inversion of well logs are the outputs of the first inversion step and are used for rock typing. The second inversion produces volumetric concentrations of rock components, subsequently used for verification of rock types. The inversion process is referred to as ‘nonlinear inversion’; Appendix A briefly explains the nonlinear inversion method implemented in this thesis

2.2.1 Bed-Boundary Selection

The concept of stacked bedding is representative of geological depositional processes in sedimentary rock, including organic shale, in the absence of folding and other tectonic alteration. Conventional multi-mineral solvers perform a point-by-point inversion through a defined interval. Nonlinear inversion as implemented in this thesis first performs inversion to estimate bed-by-bed properties from the collection of point-by-point measurements within a layer model. The basis of the layering model should be chosen from the well log with the highest vertical resolution; corresponding responses from all other logs should be included in the same bed. Figure 2.2 shows the hypothetical application of bed boundaries (dashed green lines) to field measurements overlain on a high-resolution formation image (FMI).



Figure 2.2: Well logs underlain with the corresponding electrical image log (FMI) and hypothetical bed boundaries (dashed green lines). Logs are arranged in order of highest to lowest vertical resolution from left to right. Track 1: Depth. Track 2: Resistivity and formation image. Track 3: Gamma ray and formation image. Track 4: Neutron porosity (in limestone units) and formation image. Track 5: Bulk density and formation image.

2.2.2 Mineral Model Development

A review of quantitative mineral analysis from X-ray diffraction (XRD) was used to determine the mineral model and provide a reference for inversion results. The mineral model assumes that matrix minerals, clay, and kerogen are part of the solid portion of rock, and gas and water share the pore space as fluid components. Clay may be a fixed-ratio mixture of more than one clay mineral. Each component must be assigned a molecular composition, density, etc. Kerogen is a complex and highly variable molecule, even within the same formation. Table A.1 lists the formula assumed for kerogen in this thesis (Yen and Chilingarian, 1976).

2.2.3 Inversion Results

The first step in the inversion process estimates true layer properties from input logs. Input logs are density, neutron porosity, resistivity, and PEF. Estimates of true layer properties are formation bulk density, neutron migration length (L_m), true resistivity (R_t), and PEF. The second step in the inversion uses the estimates of true layer properties to further estimate mineralogy, porosity, and saturations based on an assumed mineral model. Even when diligently performed, inherent drawbacks of multi-mineral inversion are:

- the assumption of mineral constituents in the reservoir,
- non-uniqueness of solutions, and
- under-determined formulations of the multi-mineral model.

Multi-mineral models are often calibrated to core-derived saturations and mineral compositions. The mineral model assumption constrains the solution to include elements that may not be present in the formation and may discount the contribution of minerals which may have an impact on the accurate determination of rock properties. Rock typing can be employed as an alternative method or for verification of a multi-mineral solution.

2.3 CORE RELATIONSHIPS AND LOG-BASED ROCK TYPING

Core relationships with well logs provide the geological basis necessary for developing results from log-based rock typing. The parameters of interest regarding reservoir storage capacity in shale gas wells are typically kerogen/TOC concentration, porosity, and gas saturation. Heterogeneity of rock compositions, even between wells in the same play, make core correlations a crucial step to understanding associations between measured properties within an individual well. Relationships between laboratory-measured core properties provide a connection to the interpretation of petrophysical properties from field measurements. In other words, core data provide petrophysical viability to groupings inferred from well log data.

2.4 ROCK TYPING

Cluster analysis is a statistical technique used to determine groupings in data. This technique was applied with a commercial software package, Interactive Petrophysics™, which utilizes the k-means method widely used for similarity grouping. MacQueen (1967), the first author to term ‘k-means’ clustering, explains the intended use of this method:

The point of view taken in this application is not to find some unique, definitive grouping, but rather to simply aid the investigator in obtaining qualitative and quantitative understanding of large amounts of N-dimensional data by providing him with reasonably good similarity groups. The method should be used in close interaction with theory and intuition.

As with many statistical techniques, inappropriate usage can lead to unreliable results. A geological interpretation should, ideally, accompany rock typing to make sure that the detection of groups is performed in the same depositional environment. Without knowledge of the depositional environment, an initial cluster analysis can be performed to identify an appropriate reservoir interval. Choosing a depth section in the same depositional environment is crucial to ensure that a grouped analysis is applicable since different depositional environments have unique well-log signatures (Zinsner and Pellerin, 2007). The extent of the depth interval should be small enough to avoid including bias from depth effects on log responses. However, the depth interval should be long enough to ensure a sufficient sample size.

The number of clusters, or groups, that are specified should be grounded in some geological knowledge of the formation. We assume that rocks with similar compositions and characteristics should fall into groups upon a detailed application of cluster analysis. The number of groups can be chosen from *a priori* knowledge, geological studies, or from a minimization of cluster randomness. In this thesis, the number of cluster groupings was adjusted in the process of the analysis to verify the stability of results. The goal of cluster analysis is to seek structures in large amounts of data rather than imposing structure. To this end, large numbers of variable dimensions (in this case the number of well logs) were avoided in the study.

Factor analysis was applied to reduce the dimensionality, or specifically the plurality, of well logs used for cluster analysis. MATLAB[®] contains functions which can perform factor analysis within its Statistics Toolbox[™]. This method assumes that a multivariate set of data has a relationship with an inexplicit underlying factor, referred to as a latent factor. Factor analysis attempts to exploit patterns of covariance between the measured data; measurements that are highly correlated are likely influenced by the same factors (DeCoster, 1998). Factor analysis proved useful for two purposes: (a) determining which logs should be used for cluster analysis, and (b) confirming that the inversion uses logs which respond to unique elements in shale gas.

If resistivity and sonic logs are used in the cluster analysis, it is important to address the nonlinear response inherent to these measurements. K-means cluster analysis is best performed when data correlations are linearized. Sonic slownesses and resistivity logs often display nonlinear correlations with other well logs. These correlations can be linearized by either taking the inverse of sonic and/or resistivity (returning to electrical conductivities and sonic velocities) or by taking their logarithm.

2.5 ROCK TYPING VALIDATION WITH ROCK COMPOSITIONAL RESULTS FROM INVERSION

Rock-composition estimates from nonlinear inversion provide an opportunity for the evaluation of rock types determined from well logs and inverted bed-property estimates. These compositional estimates are used to show that clustered log responses (rock types) group together because of compositional similarities, especially kerogen concentration. Rock types are then further developed and categorized; core data provide substantiation for the proposed rock types.

Chapter 3: Synthetic Case

A synthetic case was generated to explore: (a) the effect that averaging of bed-level properties has on well logs and subsequent well-log-based rock types, (b) the benefits of inversion for resolving properties in well logs and mineral compositions, and (c) what extent of data manipulation (un-inverted well logs, inverted well log properties, inverted mineral compositions) produces the most practical inputs for rock typing. The model assumes that individual beds in a formation are homogeneous and horizontally layered. Beds are often layered horizontally in shale gas, particularly those encountered in the Barnett and Haynesville shale formations, which are field examples in this thesis (Chapter 4).

3.1 DEVELOPMENT AND RESULTS OF THE SYNTHETIC CASE

The synthetic case consists of a model populated with hypothetical layer compositions; composition is constant within each layer. These compositions have a unique set of physical properties that correspond to lithology, fluid components, and environmental conditions. Physical properties of interest in this synthetic case are density, photoelectric factor (PEF), apparent deep resistivity, and migration length. Well logs were numerically simulated at a sampling rate of 0.5 ft to represent measured bulk density, neutron porosity, apparent resistivity, and PEF. Table 3.1 summarizes the volumetric concentrations of the solid and fluid constituents assumed in the model. These parameters represent compositions of hypothetical rock types: a calcite-rich rock type (type 1), a silt-rich and organic-poor rock type (type 2), and an organic-rich rock type (type 3). Rock compositions in this model are based on observations from core data in the lower Barnett formation.

Lithological Components (%)	Rock Type 1 Calcite Rich	Rock Type 2 Silt Rich	Rock Type 3 Organic Rich
Quartz	35.5	61.0	53.0
Calcite	35.5	3.5	3.5
Pyrite	1.5	1.5	2.0
Illite	24.0	24.0	24.0
Kerogen	1.5	5.0	10.5
Pore Components (%)			
Porosity	2.0	5.0	7.0
Water Saturation	80.0	40.0	20.0
Methane Saturation	20.0	60.0	80.0

Table 3.1: Hypothetical solid and fluid constituents for three rock types included in the shale gas synthetic model. Volumetric concentrations of all lithological components plus porosity sum to 100 %. Water and methane saturations are displayed as a percentage of pore space concentration.

Numerically simulated logs from the synthetic example were inverted to assess the ability of inversion to reproduce model properties at different bed thicknesses. Figure 3.1 shows the increase in error between inverted and model properties associated with decreasing bed thickness. This error confirms the impact of sampling rate on inversion results. Inverted values are unreliable estimations of true bed properties when bed thicknesses are equal to or thinner than the sampling rate. As a result, inverting well logs in thin beds gives rise to large errors on inverted values due to bed thickness and bed placement. The benefit of performing inversion, however, is to reduce shoulder-bed and vertical-resolution effects enough to emphasize layer properties which can subsequently be used for statistical grouping.

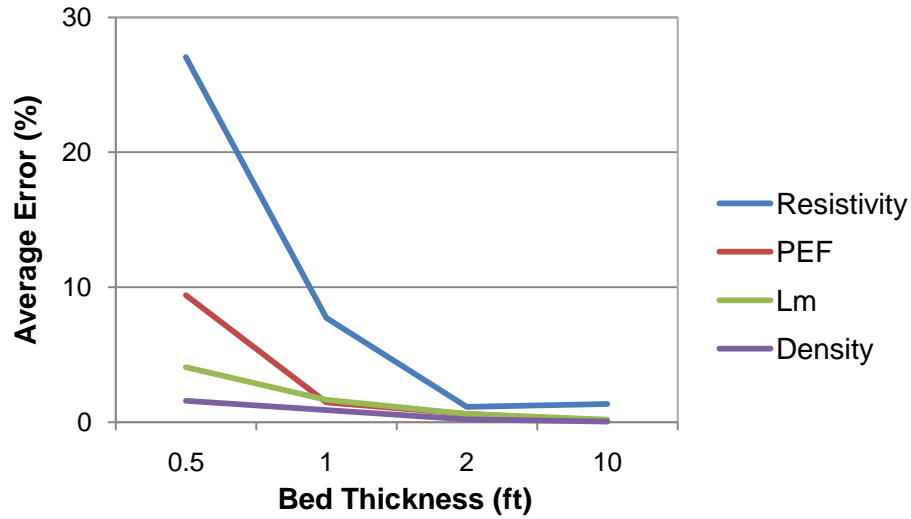


Figure 3.1: Synthetic model: average error between inverted and model properties over individual sections of 0.5, 1, 2, and 10 ft bed thicknesses. Tool resolution and sampling rate cause the error to increase with decreasing bed thickness.

The statistical grouping technique used in this thesis is k-means cluster analysis. Figure 3.2 shows the bed thickness for the corresponding model properties in the first track. Model properties are neutron, density, PEF, and resistivity. Simulated, center-bed, and inverted values are displayed on the track for the respective property. K-means cluster analysis was performed with neutron, density, PEF, and resistivity. The last four tracks of Figure 3.2 show resulting cluster-analysis groupings for the actual (model) rock types, inverted properties, center-bed values, and simulated logs. Model rock types are reproduced in order from most to least accurate: inverted properties, center-bed values, and un-inverted well logs. Inverted well-log values identify the actual rock type in beds thicker than 0.5 ft. Center-bed values return the correct rock type until the 1 ft section. Simulated logs, which represent field logs, produce groups which are a result of thin-bed and/or shoulder-bed effects in multiple instances throughout the 10 ft, 2 ft, 1 ft, and 0.5 ft sections.

Multi-mineral inversion rock-composition results give the attractive prospect of classifying rock types based directly on estimated mineral and fluid components. If concentrations of rock compositions could be estimated accurately, rock components could be

selected and classified to synthesize rock classes closely associated with geological facies. Cluster analysis for rock typing from compositional estimates is performed with kerogen, porosity, and quartz. Figure 3.3 shows bed thickness for the corresponding model properties in the first track. Model compositions shown in the second track consist of the mineral and fluid constituents that define the three different rock types shown in the third track. Track 4 shows the mineralogy inverted from an even-determined solution. An even-determined solution is generated with a number of unique inputs (well logs) to determine an equal number of outputs (rock components). Seven well logs were simulated from a model and include spectral gamma ray (Thorium, Uranium, and Potassium), resistivity, PEF, neutron porosity, and bulk density. The seven shale components in the solution are volumetric concentrations of quartz, calcite, clay, kerogen, pyrite, gas, and water. It is found that the even-determined solution yields an accurate estimation of mineral compositions and rock types. An under-determined solution, shown in track 6, has a larger number of outputs than unique inputs. The rock-compositional estimates for the field cases (Chapter 4) are under-determined problems; the number of minerals generated in the solution is in excess of the number of well logs used to determine them. In order to illustrate a typical field estimation problem, an under-determined solution is displayed in the last two tracks of Figure 3.3. Well logs input to nonlinear inversion for the under-determined case are resistivity, PEF, neutron, and density. Volumetric concentrations estimated in the inversion are quartz, calcite, clay, kerogen, pyrite, gas, and water. The accuracy of inverted estimates is poor when compared to the actual mineralogy shown in track 2.

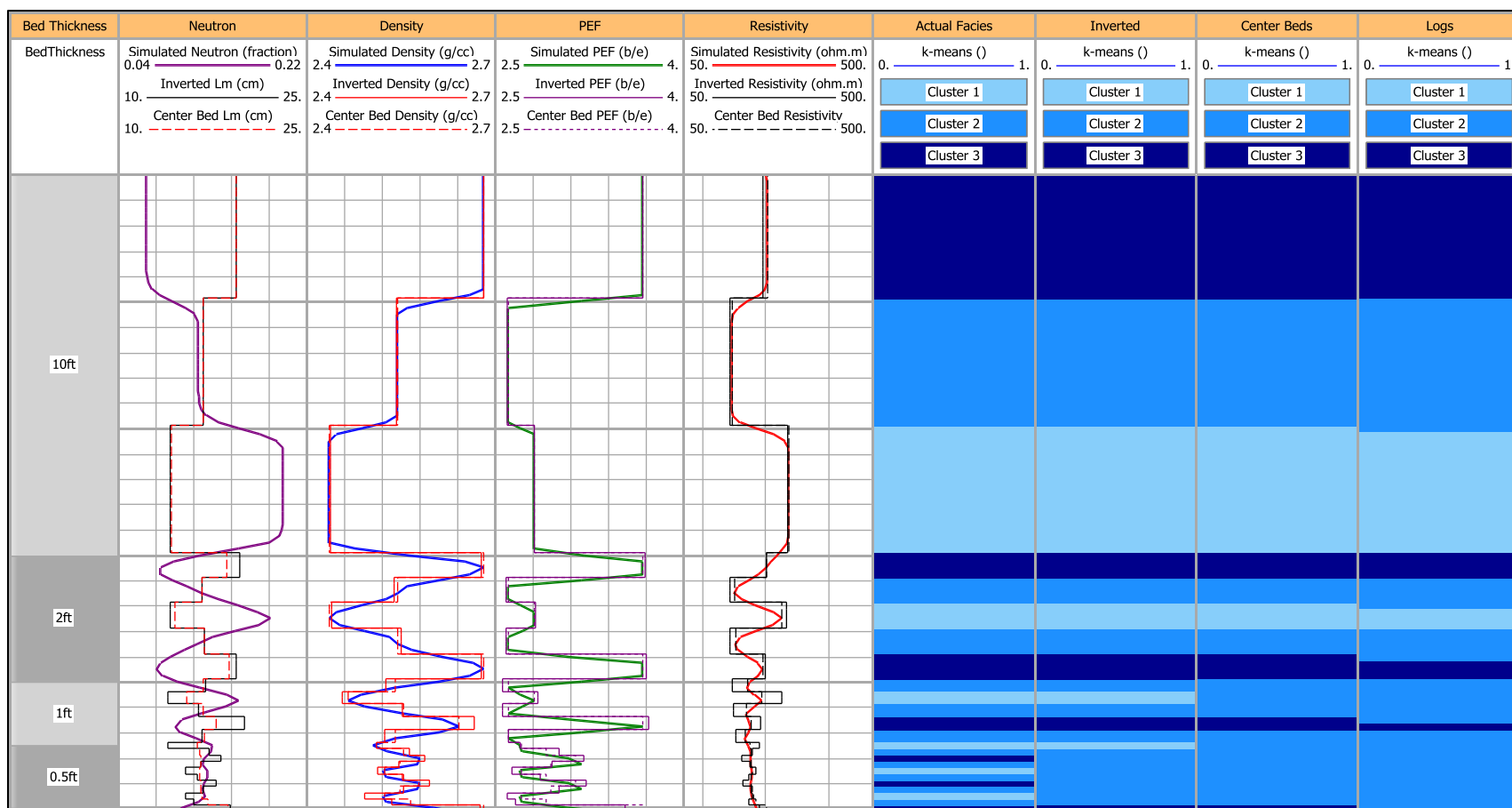


Figure 3.2: Synthetic case showing the progression from thick beds to thin beds and the associated well logs. Track 1: Bed thicknesses for the corresponding interval in a progression from 10 ft beds to 0.5 ft beds. Tracks 2–5: Simulated, model, inverted, and center-bed values for neutron porosity (limestone units), bulk density, PEF, and resistivity, respectively. Tracks 6–9: Cluster analysis results for actual rock types obtained from inverted properties, center-bed values, and log values.

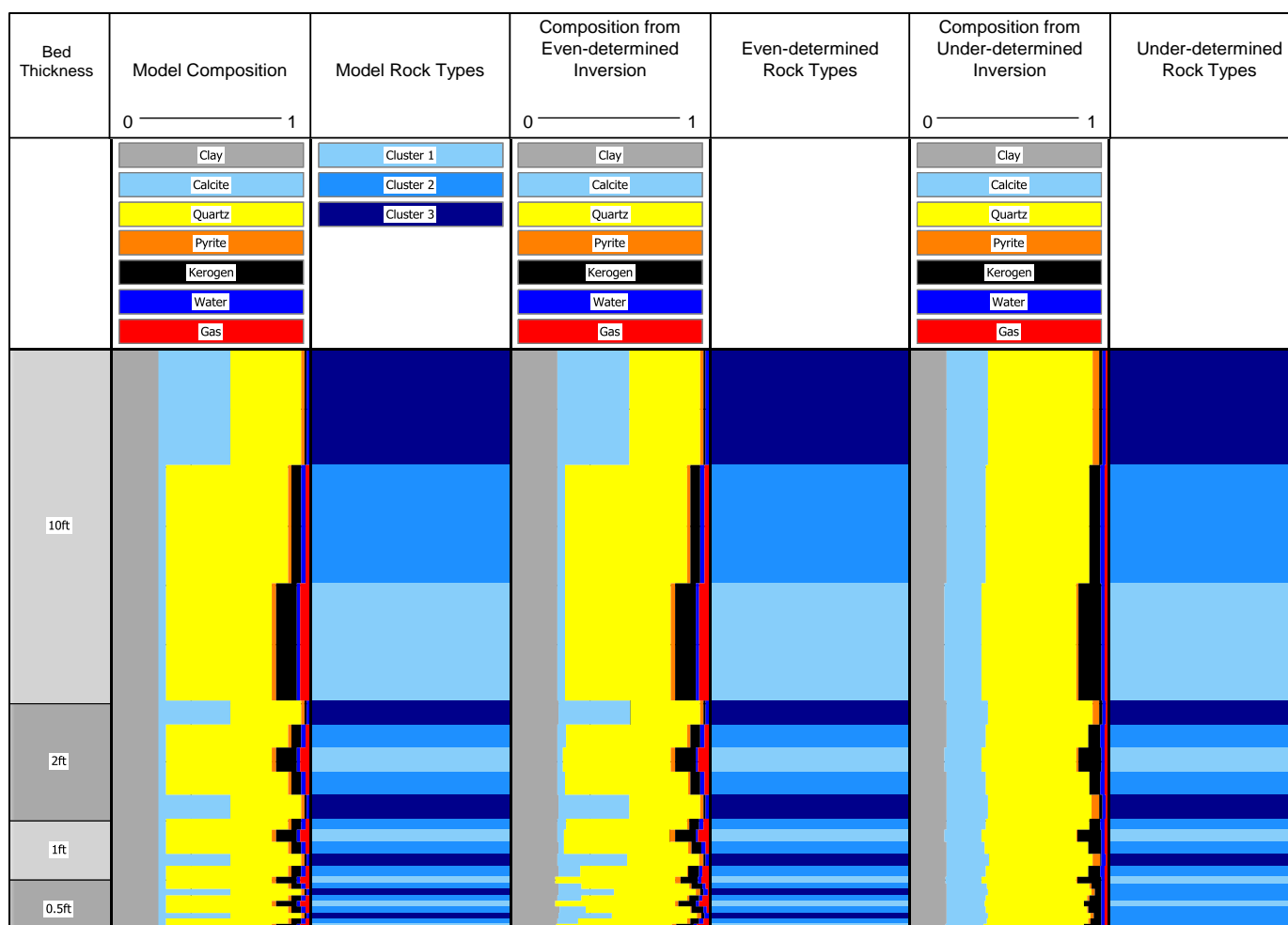


Figure 3.3: Synthetic case: multi-mineral inversion rock typing with model rock types, an even-determined solution, and an under-determined solution. Track 1: Bed thicknesses within the interval. Track 2: Model composition. Track 3: Model rock types. Track 4: Rock-compositional estimates for an even-determined solution. Track 5: Rock types determined from k-means cluster analysis based upon estimated mineral compositions in Track 4. Track 6: Rock-compositional estimates from an under-determined solution. Track 7: Rock types determined from k-means cluster analysis based upon estimated mineral compositions shown in Track 6.

Table 3.2 shows the average errors between model composition and each of the estimated mineral components for one- and two-foot beds. The even-determined solution exhibits small errors, approximately 10% or less, for all mineral components. In contrast, the under-determined solution yields large errors for most minerals, especially calcite, which is highly variable between beds.

Lithology	Even-determined Error (%)	Under-determined Error (%)
Quartz	4.3	23.0
Calcite	11.4	330.6
Pyrite	6.5	99.4
Clay	1.0	22.7
Kerogen	6.3	18.0
Porosity	8.0	37.5

Table 3.2: Average error between model mineralogy and inverted mineralogy for even- and under-determined problems.

Results from the under-determined case make an important point about the unique composition of kerogen. Kerogen has the least amount of error amongst the other minerals for the under-determined case. The chemical composition of kerogen (Appendix A) is unique because it has the lowest density and highest hydrogen index of any solid constituent. These properties relate to the overall bulk density and migration length which determine bulk density and neutron porosity well logs. The uniqueness of kerogen composition compared to that of other minerals in the model facilitates its quantification in the inversion process. As a result, even though kerogen concentration is in error, the relative concentration remains an accurate representation of the original model (Figure 3.3, tracks 2 and 6).

3.2 APPLICABILITY TO LOG-BASED ROCK TYPING IN THE FIELD

The synthetic case presented here has applicability to rock typing with field measurements. Using cluster analysis directly on well logs or their corresponding inverted petrophysical properties (Figure 3.2) indicates that log properties can be used to identify rock types. Well logs and their corresponding rock types are susceptible to error from shoulder-bed effects and tool resolution, especially in thin beds. However, bed boundary locations in field cases may not always be perceptible and can skew rock typing in both inverted petrophysical properties and inverted rock-composition estimates. Due to the large errors displayed in estimated compositions for the under-determined case and heavily model-dependent requirements of the inverted rock composition solution, rock typing between logs and their inverted properties appears more practical. Table 3.3 summarizes the advantages and disadvantages of rock typing based on the three levels of data refinement from conventional well logs.

	Advantages		Disadvantages	
Well Logs	No data manipulation		Shoulder-bed effects and averaging	
Inverted Bed Properties	Mineral-model independent method of log refinement	Reduce impact of shoulder-bed effects and averaging		<ul style="list-style-type: none"> • Placement of bed boundaries • Reduction of sample size • Propagates and magnifies errors
Inverted Mineralogy	Intuitive grouping		Introduces additional dimensions to an already under-determined problem	

Table 3.3: Advantages and disadvantages of rock typing when using different levels of data refinement.

Chapter 4: Field Examples of Rock Typing

Chapter 4 shows results from two field examples using the rock typing method described in Chapter 2. The first field example applies the rock typing method to a well in the Barnett shale gas play, while the second field example applies the method to a well in the Haynesville shale gas play. Both field examples were implemented in depth-intervals where hole quality and tension pulls had minimal impact on well logs.

4.1 FIELD EXAMPLE: BARNETT SHALE GAS PLAY

This section begins by introducing the location of the study well together with the corresponding geological and geochemical background. Core data correlations were related to well logs for the purpose of identifying the characteristics that constitute the best rock types. The most representative logs are chosen for rock typing based on factor-analysis results. Rock typing is performed using k-means cluster analysis. Resultant rock types are validated with inversion results. The section concludes with a comparison between conventional methods for TOC quantification and its implications in rock typing.

4.1.1 Geological and Geochemical Background

Recently, the Barnett formation has been used as an exploration model for many emerging shale gas plays. The well used in this study is a vertical pilot hole which penetrates the Barnett formation close to its thickest stratigraphic extent along the Muenster Arch. A basinal depositional environment was interpreted by a commercial core laboratory for the study area in the lower Barnett formation. The lower Barnett formation is the focus of this study since it is the most thermally-mature interval and, consequently, the most likely to be commercially productive. Common measures of kerogen maturity — vitrinite reflectance (R_o) and calculated maturity (via pyrolysis) — average 0.89 and 1.12, respectively. Thermal maturities from cored samples in the lower Barnett formation indicate a reservoir which has not matured completely. Corresponding gas/oil ratios range from 2.5 to 17.4, as determined by laboratory core measurements.

Papazis (2005) identified five lithological groups from a core study in the Barnett formation: black shale lacking in silt-size particles, silt-rich black shale, calcite-rich lithologies, coarse grain accumulations, and concretions. The core description produced by a professional core laboratory described similar features.

4.1.2 Log Response and Rock Property Relationship

Core measurements in this well show a strong correlation between volumetric concentrations of kerogen, porosity, and water saturation. Figure 4.1 shows the relationship between kerogen concentration, porosity, water saturation, and bulk density. Core bulk density trends toward lower values with increased kerogen concentration, porosity, and gas saturation. Figure 4.1 also shows a formation image from a thinly-bedded interval and a high-resolution bulk density log which emphasizes the low-densities of many of the thin beds. This behavior indicates that layers with the lowest densities have the highest kerogen concentration, porosity, and gas saturation.

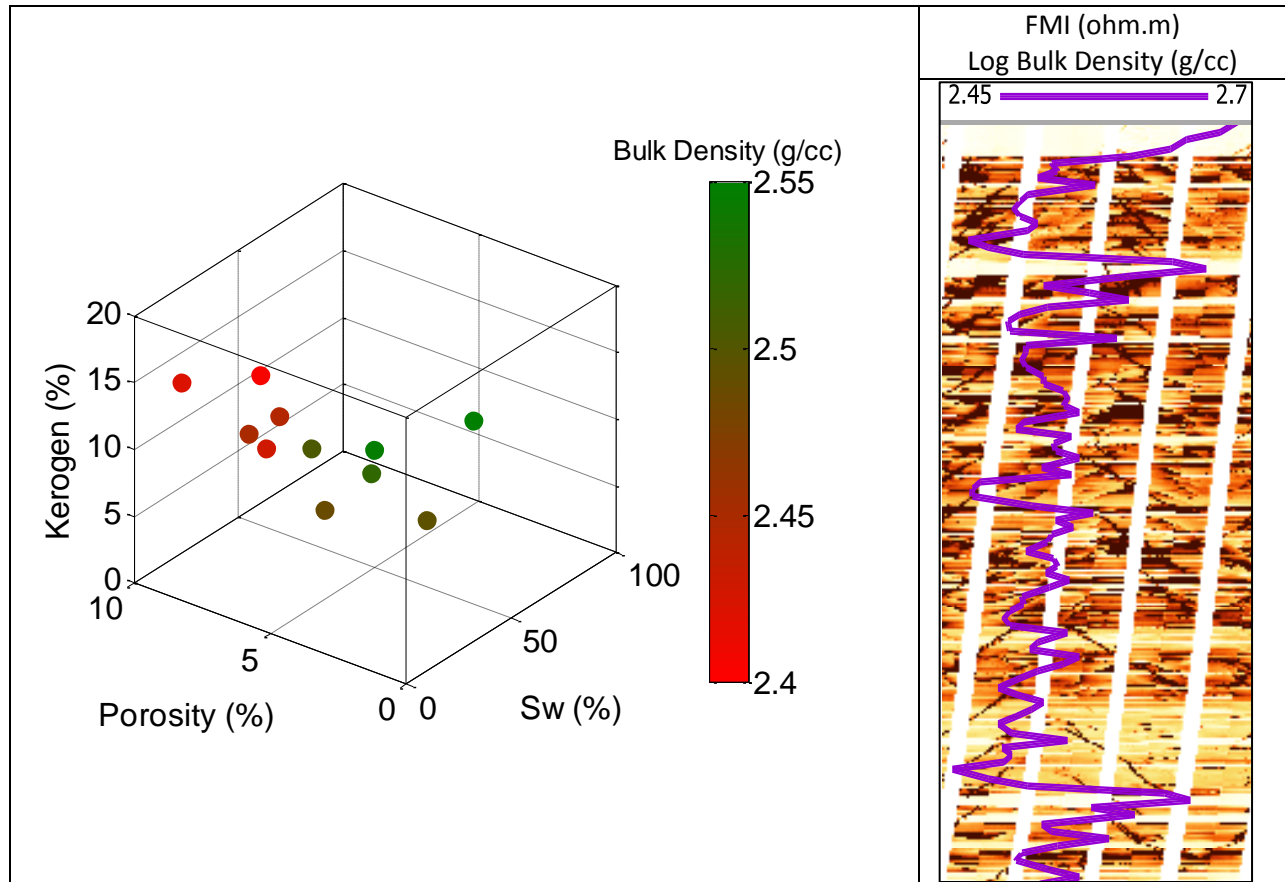


Figure 4.1: The three-dimensional cross-plot shows the relationship between core-measured kerogen (volumetric percent), porosity (volumetric percent), and water saturation (S_w , percent of pore space); the color scale indicates the corresponding core-measured bulk density. The log track (right) shows a formation image overlain by the bulk density well log.

Factor analysis was then used to reduce the dimensionality of available well logs. Figure 4.2 shows a biplot of factor-analysis results performed in an organic- and gas-rich interval. Two latent factors were imposed for 2-dimensional visualization of groupings, which are evident in this case. Since factor analysis serves the purpose of identifying overlapping measurements, its importance lies in how the projections group rather than the latent factor value shown in Figure 4.2. Groupings provide quantitative indication that well logs respond to separate factors in the shale under consideration and are appropriate for segregating different rock types. Furthermore, bulk density and PEF can be interpreted to have a significant relationship to shale-matrix components. Neutron porosity, sonic, and gamma-ray logs can be interpreted as having

dependency upon concentrations of organic matter and/or fluids in the pore space. Resistivity can be interpreted to have a relationship with fluid saturation, conductive minerals (pyrite), and conductive clays (smectite). The highest resolution logs from each grouping— resistivity, density, and neutron—were used in the application of k-means cluster analysis.

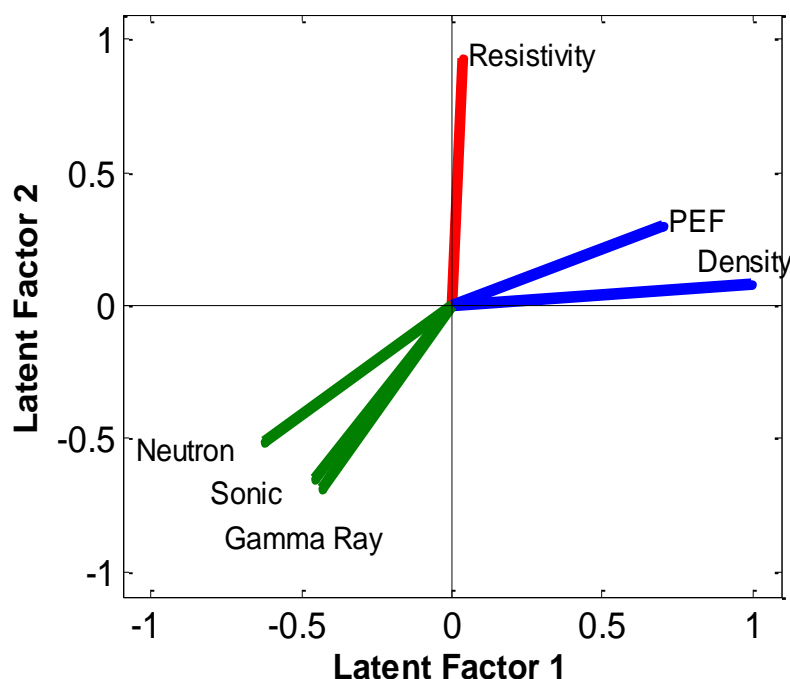


Figure 4.2: Biplot for factor analysis for the lower Barnett formation. Projections are labeled with the corresponding well logs. Colors designate statistically significant relationships between groups of well logs. The projection labeled ‘Sonic’ refers to compressional sonic slowness.

4.1.3 Rock Typing in the Lower Barnett Formation

Depth bounds for the rock typing interval were chosen based on the core interval. The entire depth interval (90 ft) belongs to a basinal depositional environment. Core data indicate the presence of an organic rich rock type with high porosity and gas saturation. Cluster analysis was employed to explore associations between log data that would suggest a low density cluster corresponding to a group suggestive of gas- and organic-rich rock. Papazis (2005) suggested the presence of five lithofacies and Kale et al. (2009) suggested the presence of 3 petrophysical

facies, both applicable to the Barnett formation. The appropriate number of cluster groupings was narrowed, from these prior publications, to between 3 and 5 groups.

A four-element cluster minimized cluster randomness and provided a stable set of groups. The stability of groupings was determined by adjusting the number of cluster groups to observe if the solution, i.e. groupings, changed appreciably. Figure 4.3 shows cross-plots between density, neutron, and resistivity as generated by k-means cluster analysis for both the inverted log properties and well logs. Resultant clusters for inverted properties and well logs are similar to each other and identify: (a) a low-medium resistivity, low density, high neutron group shown in red, (b) a mid-range density, mid-range resistivity, mid-range neutron porosity group in green, (c) a low density, high resistivity, mid-range neutron porosity group in blue, and (d) a high density, low neutron porosity, high resistivity group in yellow. Inverted well log properties (Figure 4.3b) represent a smaller sample size and reduce shoulder-bed effects. As a result, inverted properties provide a clearer visualization of cluster groupings. This behavior confirms that the number of clusters chosen does not represent arbitrary groupings.

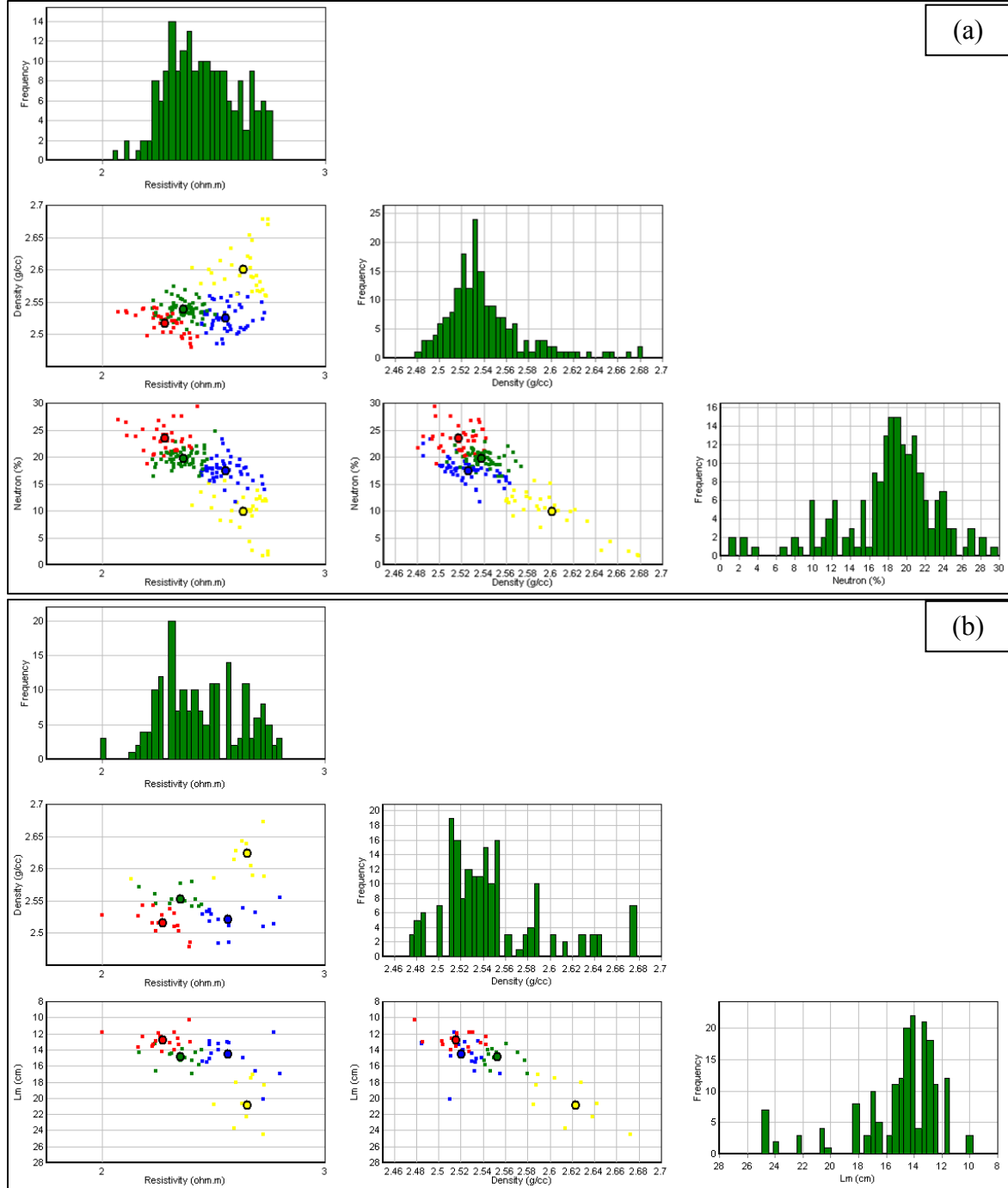


Figure 4.3: Cross-plots and histograms of cluster groupings: (a) well log measurements of resistivity, bulk density, and neutron porosity (in limestone units) and (b) inverted properties for resistivity, bulk density, and migration length (Lm).

Bulk density has been shown to exhibit correlation with kerogen concentration, porosity, and gas saturation in Figure 4.1. Also, the synthetic example (Chapter 3) indicated that neutron porosity is heavily influenced by kerogen concentration. Nonlinear inversion is used to associate rock compositions (i.e. mineral concentrations) with rock types (Figure 4.6, track 5) Table 4.1 summarizes these groups and their interpreted rock type.

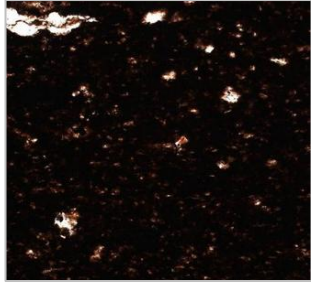
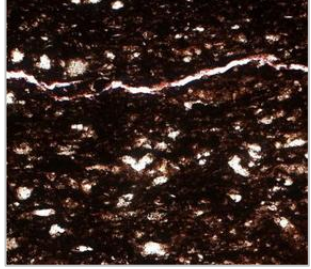
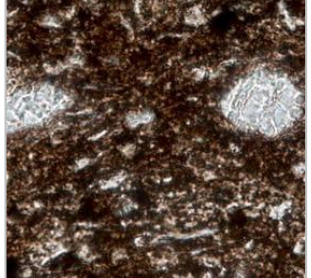
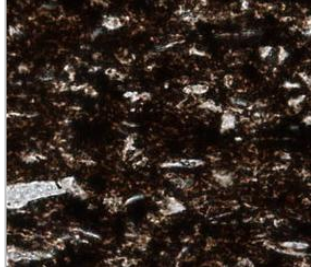
Rock Types	Log Response	Proposed Rock Type	Thin Section	Volumetric Composition (%)
Rock Type 1	Low density, high neutron porosity, low-medium resistivity	Organic rich, high porosity, high gas saturation		Gas-filled porosity: 4.48 Quartz: 46.2 Carbonate: 3.2 Kerogen: 11.1
Rock Type 2	Mid-range density, mid-range resistivity, mid-range neutron porosity	Silt rich, organic lean, lower porosity		Gas-filled porosity: 2.62 Quartz: 57.3 Carbonate: 4.0 Kerogen: 6.8
Rock Type 3	Low density, high resistivity, mid-range neutron porosity	Organic rich, high gas saturation, higher carbonate content		Gas-filled porosity: 3.89 Quartz: 46.2 Carbonate: 7.7 Kerogen: 12.2
Rock Type 4	High density, low neutron porosity, high resistivity	Non-reservoir, carbonates or concretions		Gas-filled porosity: 0.8 Quartz: 65.3 Carbonate: 20.4 Kerogen: 4.3

Table 4.1: Proposed rock types based on the cluster analysis of well logs and validated with multi-mineral inversion results. Thin section images and corresponding compositions are included for the proposed rock types.

Figure 4.4 shows the logs and inverted log values used for rock typing as well as the formation image and corresponding rock types. The formation image confirms the presence of thin beds. Below X590 ft (relative depth), the rock types alternate frequently. From the log responses and proposed rock types, the blue- and red-colored rock types likely synthesize the best reservoir properties as a result of groupings with the lowest density and highest neutron response. Rock types identified from well log and inverted well-log properties are similar. The thinly-bedded section between depths X600 and X630 ft contains the largest number of depth samples belonging to rock type 1. Rock type 1 occupies 40% more reservoir height with the inverted-property rock types than with well-log-based rock types over the entire 90 ft depth interval.

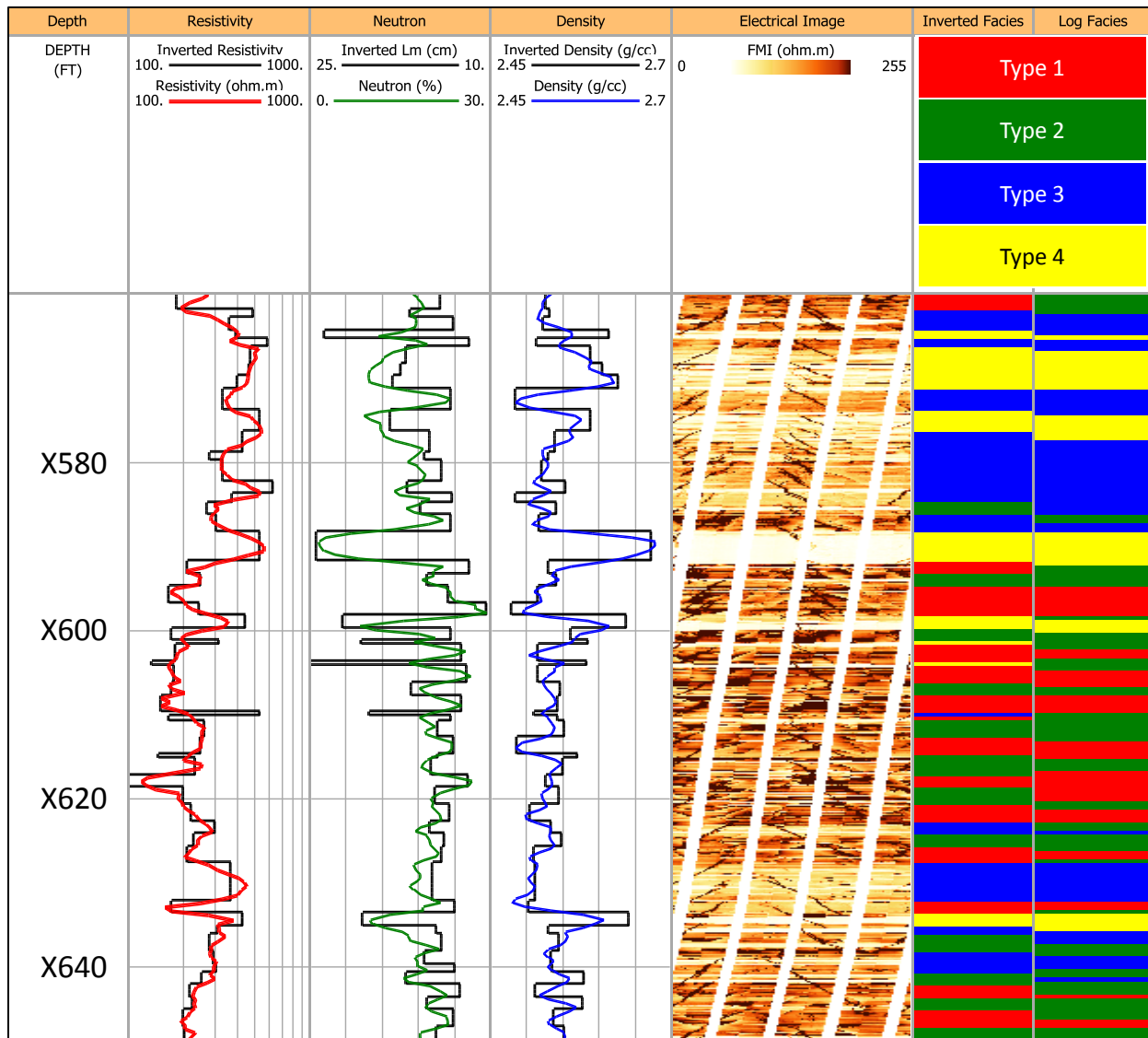


Figure 4.4: Inverted log properties, formation image, rock typing, and mineralogy. Track 1: Relative depth. Track 2: Apparent resistivity and inverted resistivity. Track 3: Neutron porosity (in limestone units) and inverted migration length. Track 4: PEF and inverted PEF. Track 5: Bulk density and inverted density. Track 6: Electrical image. Track 7: Log-based rock types. Track 8: Rock types from inverted properties.

Kerogen concentration was the least error-prone inverted rock component from the synthetic case (Chapter 3). Because core correlations show a positive trend between kerogen concentration, porosity, and gas saturation, inverted kerogen concentrations are used as a rock-quality metric. Figure 4.5 shows that interpreted rock types (Table 4.1) are valid in terms of

organic richness. Rock quality ranking in terms of kerogen concentration from highest to lowest is: (I) rock type 1, (II) rock type 3, (III) rock type 2, and (IV) rock type 4.

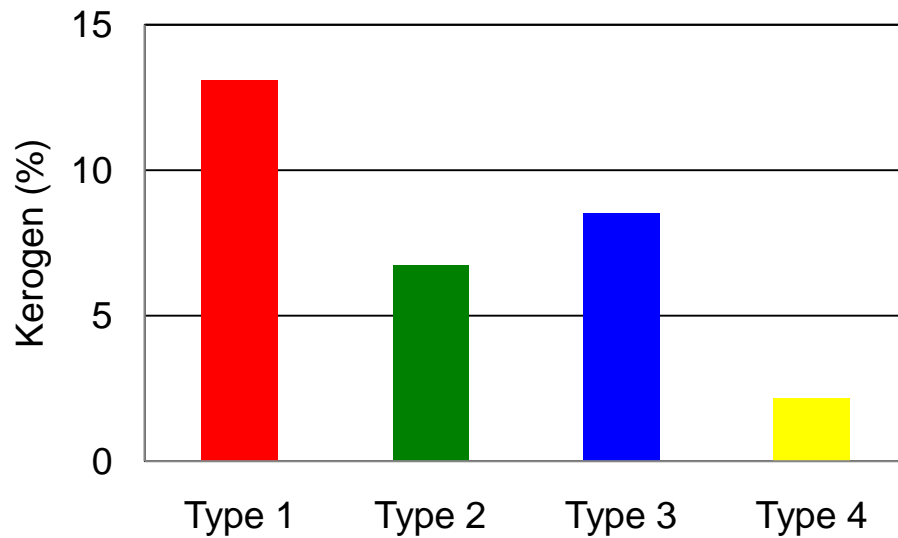


Figure 4.5: Average volumetric concentration of kerogen for different rock types; kerogen concentration is estimated with nonlinear inversion.

4.1.4 Significance of Resolution and Rock Typing

Conventional methods and commercial software tend to show average values of kerogen and saturation across a given depth interval. Most conventional quantitative evaluations of organic shale use multiple logs without correction for shoulder-bed effects and depth of investigation. Furthermore, lower-resolution logs such as sonic and resistivity can obscure the presence of thin beds. Figure 4.6 shows well-log-based rock types compared to inverted TOC, TOC from Passey's method (Passey et al., 1990), and core TOC. Additionally, nonlinear inversion rock-composition results are compared to results obtained with a commercial software. Figure 4.6 shows the likelihood that the rock types identify compositionally similar rock types that suggest an organic-rich/organic-poor alternating sequence. Results from conventional techniques suggest a more homogeneous section with less frequent rock-composition variation with depth.

Passey's method is calculated from bulk density and deep apparent resistivity logs using the method introduced by Passey et al. (1990). The assumption made in Passey's formula is that the increase in kerogen/TOC concentration causes a corresponding decrease in sonic velocity or bulk density and an increase in apparent deep resistivity. The lower Barnett formation well studied in this thesis suggests that bulk density and sonic velocity decrease with increasing organic content, but resistivity does not always exhibit a corresponding increase. Such behavior may be due to the presence of fractures, undermature kerogen, and bound water that provides a conductive path with increasing pore and pore-throat space in the organic rich zone. Furthermore, Passey's method tends to yield average trends when compared to core-measured TOC. Rock types shown in the third and fourth track of Figure 4.6 identify a unique set of rock types and nonlinear inversion validates the rankings of organic richness. It is important to note that TOC concentration estimated with the multi-mineral code ('Inverted TOC', track 2) in the zone from X595–X610 ft is highly affected by noise and is therefore susceptible to error.

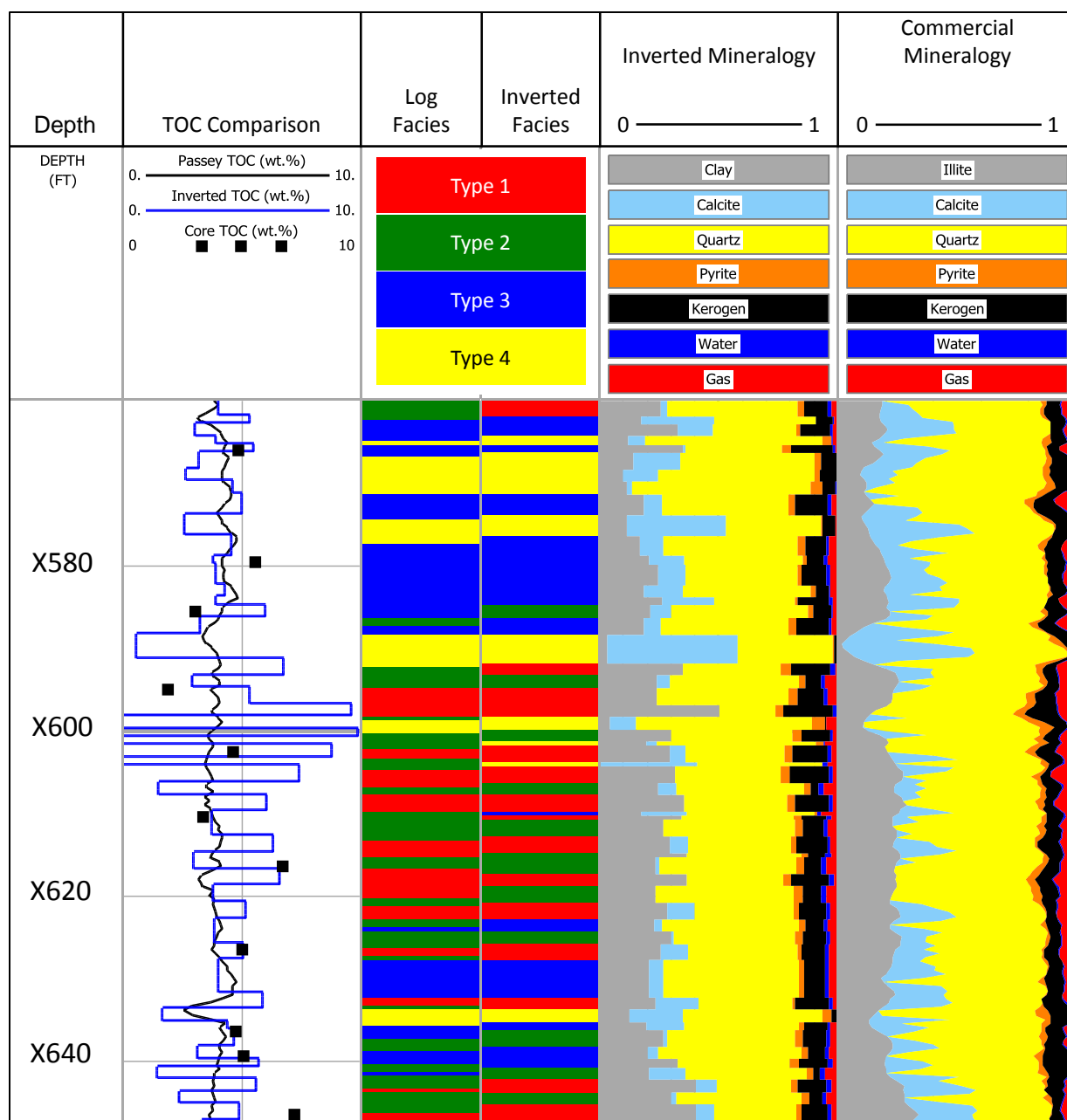


Figure 4.6: Thin beds and comparison of kerogen volumetric concentration estimated from inversion and conventional methods. Track 1: Relative depth. Track 2: Comparison of TOC derived with Passey's method (Passey et al., 1990), nonlinear inversion, and laboratory core. Track 3: Log-based rock types. Track 4: Inverted-property-based rock types. Track 5: Mineralogy estimated with nonlinear inversion. Track 6: Mineralogy estimated with a commercial linear solver.

4.2 FIELD EXAMPLE IN THE HAYNESVILLE FORMATION

This section introduces the basic geology and location of the Haynesville shale gas play. Core data are associated with well logs for the purpose of identifying specific properties that constitute the best rock types. The most representative logs are chosen for rock typing based on factor analysis. Rock typing is performed using k-means cluster analysis.

4.2.1 Geological Background

The Haynesville shale gas play is an organic-rich shale which extends areally through part of northeast Texas and northwest Louisiana. It is bounded by the Bossier shale formation above and either the Haynesville Limestone or Smackover Limestone beneath (Buller et al., 2010). The geological age of the formation is interpreted to be Upper-Jurassic (Johnston et al., 2000). The well in this study is located in Panola County, Texas. A core description for the 90 ft study interval was included in the available data. In this 90 ft interval, the core description interprets massive to faintly laminated geological facies interpreted to belong between a subtidal-slope to basinal depositional environment.

4.2.2 Well Log Response and Rock-Property Relationships

Ideally, rock classification should be performed in a specific type of depositional environment due to its unique well log signatures. This example describes the application of rock classification to a transitional zone. Figure 4.7 shows the relationship between TOC, porosity, water saturation, and bulk density throughout the entire cored depth-interval of 240 ft. As with the Barnett formation example, the figure indicates that layers with the highest TOC concentration also exhibit the highest porosity and gas saturation. Furthermore, core bulk density trends toward lower values with increased TOC concentration, porosity, and gas saturation. Figure 4.7 also shows the range of points belonging to the 90 ft study interval within a blue oval. The circled core properties are closely grouped when compared to the range of porosity, water saturation, and TOC concentrations throughout the entire cored interval.

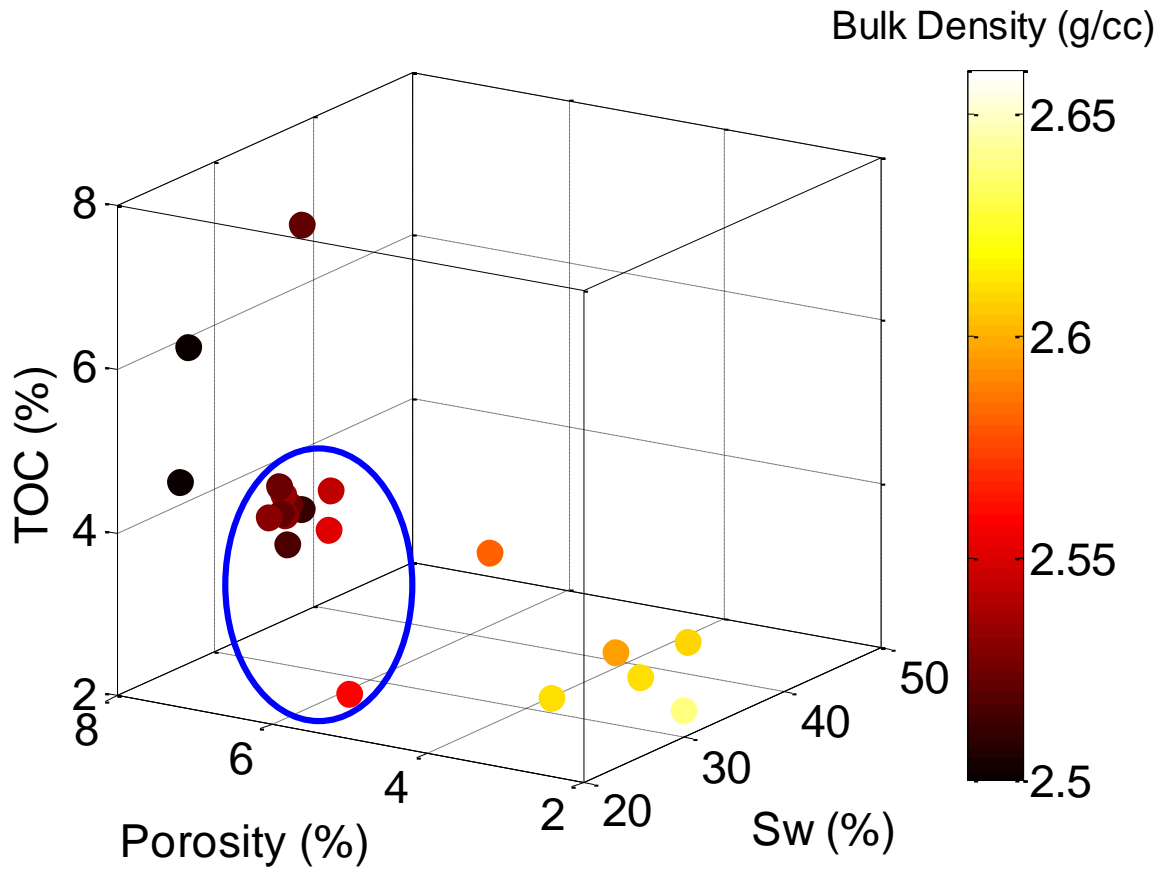


Figure 4.7: Three-dimensional cross-plot showing the relationship between core-measured TOC (weight percent), porosity (volumetric percent), and water saturation (S_w , percent of pore space); the color scale identifies the corresponding core-measured bulk density. The blue oval designates the core points within the studied depth-interval.

Table 4.2 shows the standard deviations of core data and well logs belonging to the Haynesville formation and Barnett formation study intervals. These standard deviations are computed from well logs (apparent resistivity, bulk density, and neutron porosity) and core measurements (water saturation, bulk density, TOC concentration, and porosity). The low standard deviations of the Haynesville formation—relative to the standard deviations from the Barnett formation—suggest a vertically-homogenous formation.

Core Data	Standard Deviations	
	Haynesville Formation Study Interval (90 ft)	Barnett Formation Study Interval (90 ft)
TOC (wt. %)	0.67	1.54
Porosity (volumetric %)	0.49	1.84
Water Saturation (pore space %)	2.41	18.24
Bulk Density (g/cc)	0.01	0.05

Well Logs		
Resistivity (ohm.m)	10.43	107.04
Neutron Porosity (limestone units, %)	1.82	4.90
Bulk Density (g/cc)	0.02	0.04

Table 4.2: Standard deviations of well logs used in the cluster analysis and pertinent core data (TOC, porosity, water saturation, and bulk density).

Factor analysis is used to reduce the plurality of well logs for cluster analysis. Figure 4.8 shows the results of factor analysis performed on the Haynesville formation well. Two latent factors were imposed to aid in the visualization of groupings; groupings are less distinct in the Haynesville formation application than in the Barnett formation example (Section 4.1). However, the groupings provide quantitative support for the covariance between types of well logs. Resistivity, bulk density, and neutron porosity were chosen as inputs to k-means clustering.

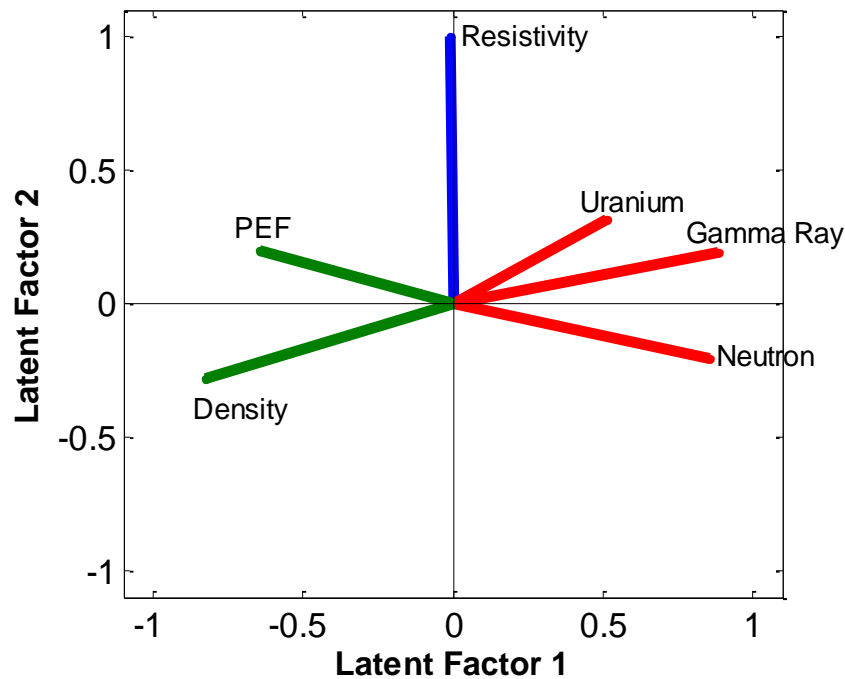


Figure 4.8: Factor analysis for the depth interval within the Haynesville shale gas play. Colors designate statistically significant relationships between logs.

Figure 4.9 shows cluster cross-plots between bulk density, neutron porosity, and resistivity. Two cluster groups were chosen to reduce cluster randomness for both well logs and inverted properties. The selection of two groups was not supported by previous studies or geological knowledge of dominant facies. However, the groupings do not appear to be unfounded based on the exhibited clustering shown in Figure 4.9. The red group (rock type 1) trends toward values of low density porosity, high neutron porosity, and low apparent resistivity. On the other hand, the green group (rock type 2) trends toward values of low neutron porosity, high density, and high resistivity. Groupings are similar between well logs (Figure 4.9a) and inverted well log properties (Figure 4.9b). Inverted well log properties represent a smaller sample size and reduce shoulder-bed effects. Consequently, inverted properties provide a clearer visualization of cluster groupings.

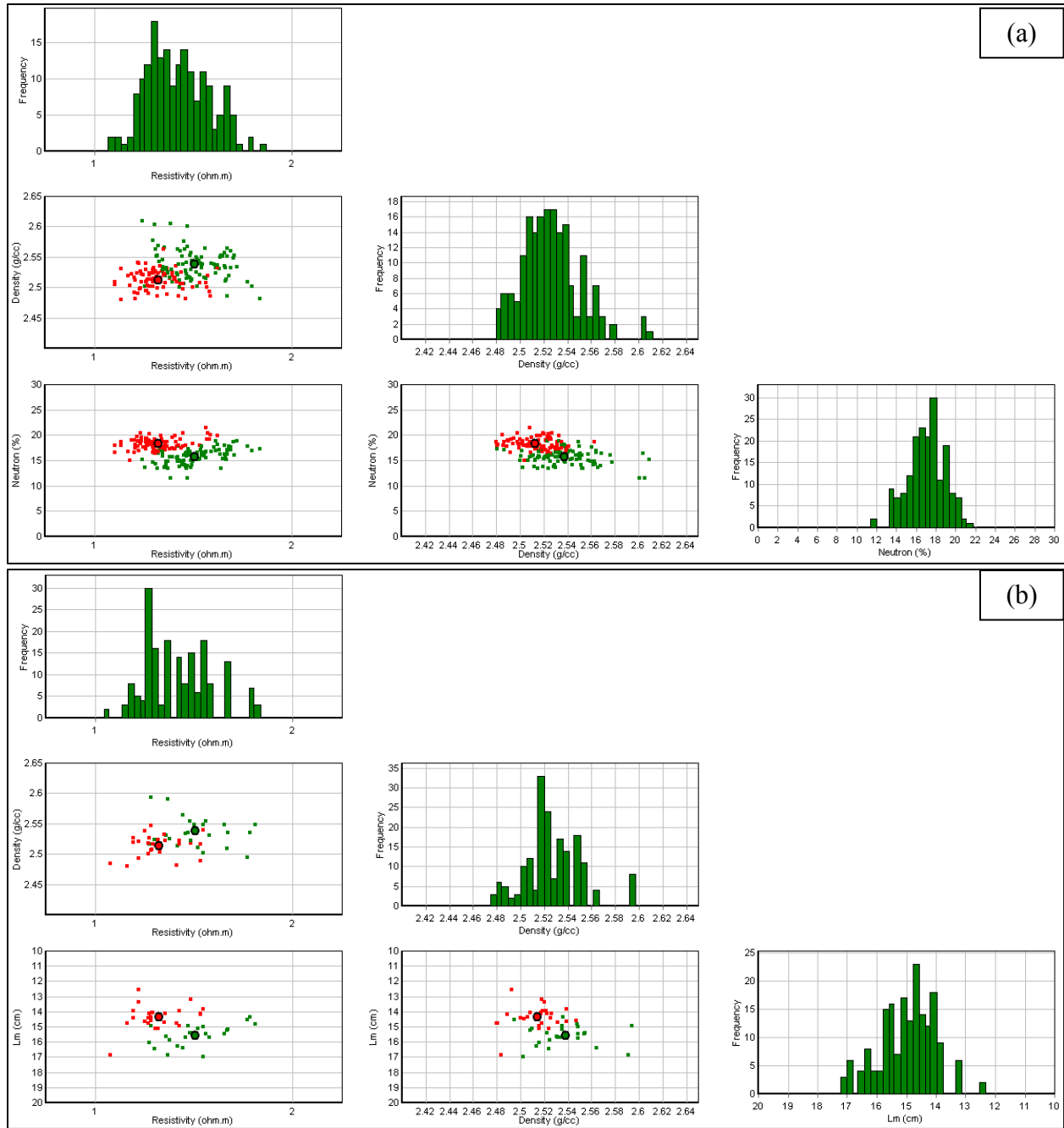


Figure 4.9: Cross-plots and histograms of cluster groupings: (a) well logs for apparent deep resistivity, bulk density, and neutron porosity (in limestone units) and (b) inverted properties for resistivity, bulk density, and migration length (Lm).

Figure 4.10 shows well logs and inverted properties, core data, and corresponding rock types within the 90 ft study interval. The core data shown do not vary widely within the interval. Well-log-based rock types and inverted well-log properties show a similar distribution pattern of

rock types with depth. From well-log-based rock types, rock type 1 constitutes 46.4% of the reservoir while rock type 2 constitutes the remaining 53.6%. For inverted well-log properties, each rock type constitutes approximately half of the reservoir. This difference may be attributed to shoulder-bed effects; however the placement of bed boundaries is often uncertain and can result in errors in rock types inferred from inverted well-log properties.

This depth interval was interpreted to belong between a subtidal-slope to basinal depositional environment based on a geological interpretation. Depositional environments impact rock attributes which, in turn, affect well logs. Table 4.3 shows the proposed interpretation of rock types. Hammes (2010) showed that TOC concentration increases distally and decreases proximally in the Jurassic. Basinal depositional environments are distal to the proximal subtidal-slope depositional environment. TOC concentration is directly related to kerogen concentration and they are both measures of organic-matter concentration. Because the average kerogen composition for rock type 1 is 1.6% above rock type 2, rock type 1 is interpreted to be associated with a distal-trending depositional environment.

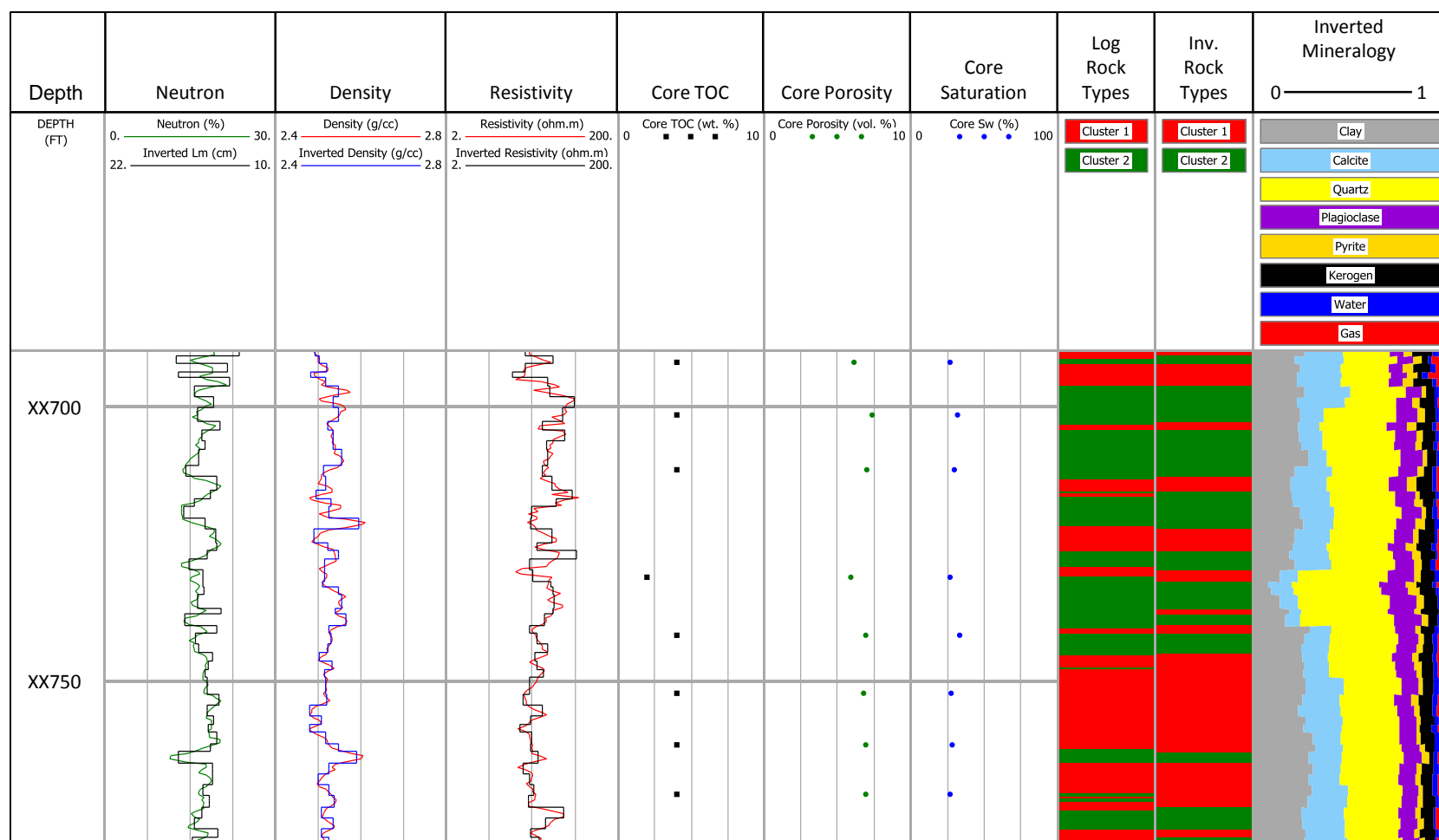


Figure 4.10: Inverted log properties and well logs, core data, rock typing, and mineralogy. Track 1: Relative depth. Track 2: Neutron porosity (in limestone units) and inverted migration length. Track 3: Bulk density and inverted bulk density. Track 4: Apparent deep resistivity and inverted resistivity. Track 5: Core TOC. Track 6: Core porosity. Track 7: Core saturation. Track 8: Rock types from well logs. Track 9: Rock types from inverted log properties. Track 10: Rock-composition estimates obtained from nonlinear inversion

Rock Types	Well Log Response	Proposed Rock Type	Proposed Depositional Environment	Average Kerogen Concentration from Inversion (Vol. %)
Rock Type 1	Low- to medium-range density, high neutron porosity, low- to medium-range resistivity	Organic rich, high porosity, high gas saturation	Distal, basinal	7.0%
Rock Type 2	Mid- to high-range density, mid- to high-range resistivity, low-range neutron porosity	Organic lean, lower porosity	Proximal, slope	5.4%

Table 4.3: Proposed rock types based on cluster analysis of well logs and inverted kerogen concentration.

Chapter 5: Discussion

This chapter addresses reservoir characteristics that were considered but not integrated into the rock typing criteria advanced in the thesis. Topics addressed are: (a) mechanical properties and their contribution to the fracture-ability of shale reservoirs, (b) fractures and their contribution to production enhancement but detriment to resistivity-log reliability, and (c) kerogen maturity and the need for high frequency core sampling to advance the shale-composition/well log connection for rock typing.

5.1 DISCUSSION ON THE IMPORTANCE OF MECHANICAL PROPERTIES AND FRACTURES

Rock classification attempts to synthesize data to extract the most significant properties with which to characterize a reservoir for hydrocarbon-production capability. Shale reservoirs require fracture stimulation and mechanical properties must be quantified to assess the reservoir's fracture potential. Petrophysical evaluations typically utilize sonic logs to perform *in situ* estimations of rock brittleness (Rickman, 2008). Associating rock mechanical properties in a way that could estimate brittleness/stimulation-potential would enrich the significance of rock classification. Core measurements provided the basis for well-log-based rock typing in this thesis. In the author's opinion, characterization of rock brittleness from sonic logs should also be based on laboratory core measurements. Specifically, confined triaxial tests should be performed to associate the resultant static Young's modulus and Poisson's ratio to dynamic mechanical properties derived from sonic logs.

Fractures may also be present prior to stimulation as a result of past or present stress fields in the form of natural or drilling-induced fractures. Both of these fracture types were identified in the course of the study. Figure 5.1 shows a rose diagram of fracture count and azimuth from drilling-induced and natural fractures within a 90 ft

study interval in the lower Barnett formation. The fracture count and azimuth was determined from an electrical image log.

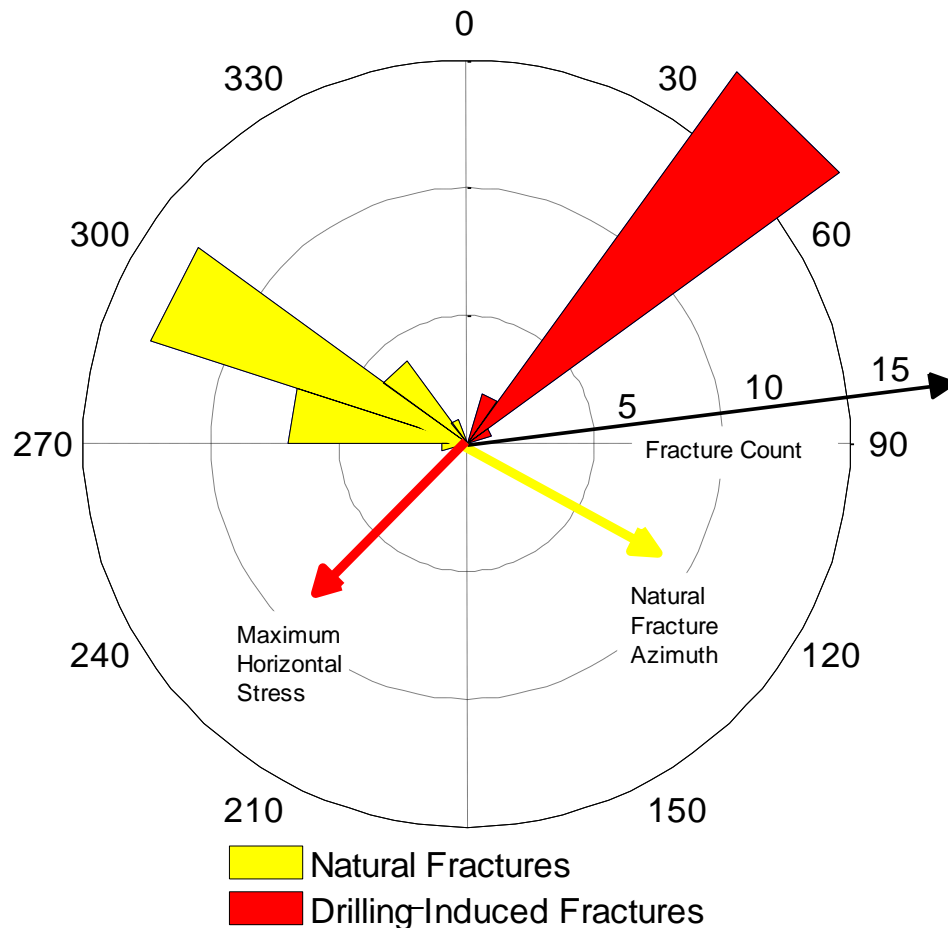


Figure 5.1: Rose diagram showing the high concentration of natural and drilling-induced fractures in the lower Barnett formation study interval (90 ft). The azimuth of drilling-induced fractures indicates the maximum horizontal stress.

Debate exists as to whether these fractures inhibit or enhance productivity (Gale et al., 2007). Fractures have importance in well-log-based rock typing for two reasons: (1) their effect on well-log quality, and (2) the effect organic matter and maturity have on fracturing. The relationship between fractures and kerogen maturity was inconclusive

from this study. Effects of fractures on well logs, especially sonic and induction resistivity logs, have been well-studied (Xue et al., 2008; Vernik et al., 2011). Figure 5.2 shows a core-slab photo with mineralized, high-angle natural fractures. The corresponding formation image displays dark (electrically conductive) sinusoidal features which are interpreted to belong to the same natural fracture type as those observed in the core-slab photo.

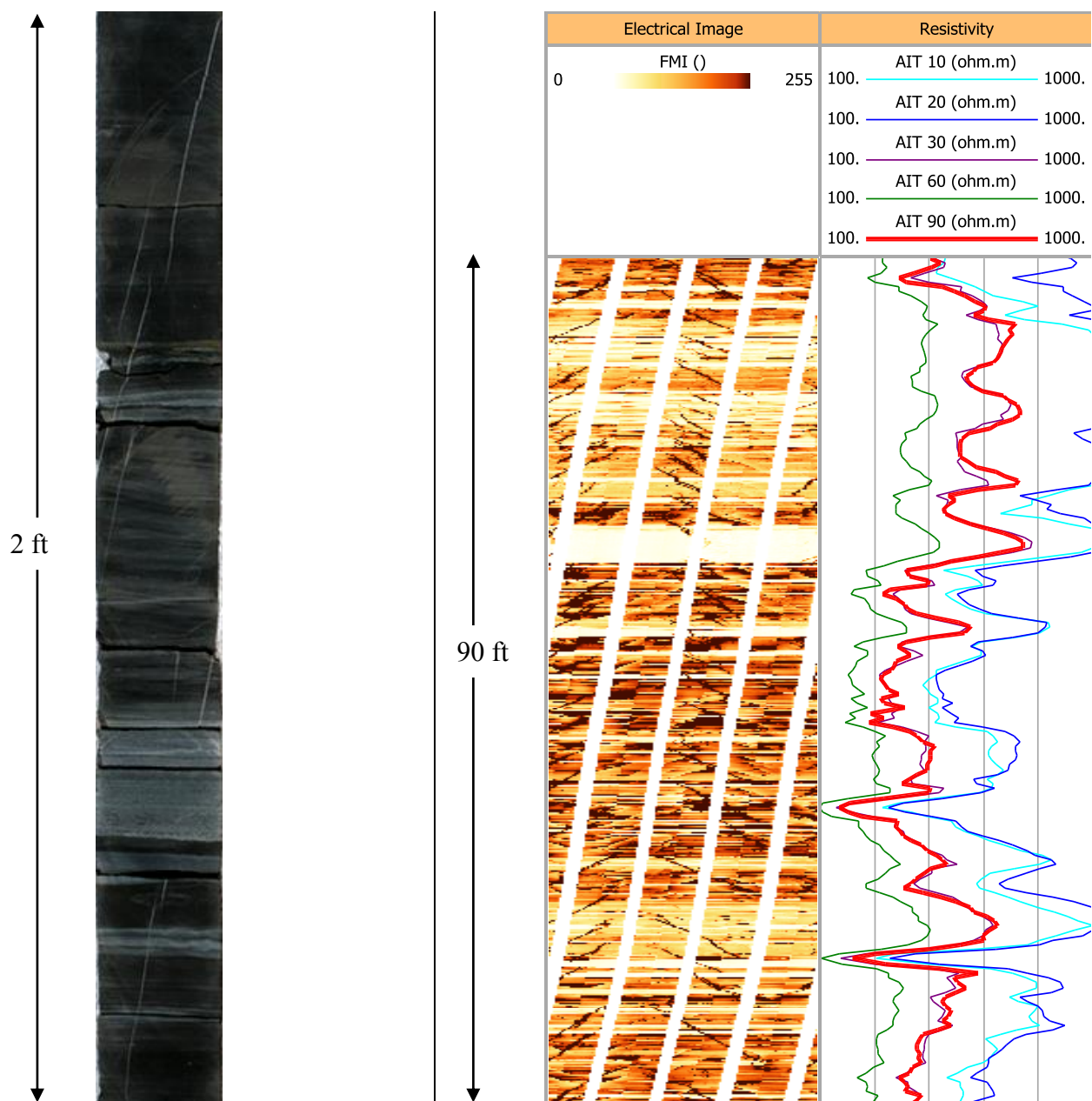


Figure 5.2: A core-slab photo (left) shows mineralized, high-angle, natural fractures. At right: Track 1 shows the electrical formation image; Track 2 shows the separation of array induction resistivity logs. The formation image displays dark (electrically conductive) sinusoidal features which are interpreted to belong to the same natural fracture type as those observed in the core-slab photo.

A comparison of the core-slab photo, formation image, and resistivity logs indicate the possibility of fracture dilation under hydrostatic pressure from drilling fluid. Mineralized fractures from the core-slab photo are sealed with calcite or dolomite precipitated and should display high resistivity in the formation image. Instead, they appear conductive in the formation image and are likely fluid-filled. Array induction apparent resistivity logs (AIT¹) measure formation resistivity at multiple radial lengths of investigation. They display characteristics of near-borehole radial alteration with indication that fractures have an effect on the measurements. The deep resistivity log (AT90) is commonly assumed to be the most representative measurement of formation resistivity in its unaltered state. This same assumption was made in this thesis.

5.2 DISCUSSION ON THE IMPORTANCE OF KEROGEN MATURITY AND CORE DATA

In addition to the effect of fractures and mechanical properties, rock classification could attempt to take kerogen maturity into account. Kerogen maturity cannot be measured directly with well logs. As a result, a large volume of the formation would have to be cored and sampled in order to perform frequent measurements on core plugs to quantify kerogen maturity. A large-scale core study could produce measurements of key rock properties (kerogen maturity, porosity, gas saturation, etc.) which could then be classified into core-based rock types. These rock types could be related to well logs for the development of a more comprehensive rock typing approach in shale gas plays. The procedures developed for this project proceeded from a limited amount of core data and were intended for practical applications.

¹ Mark of Schlumberger

Chapter 6: Conclusions

This chapter summarizes the salient conclusions of the thesis and makes recommendations for the advancement of rock typing using conventional well logs in hydrocarbon-bearing shale.

6.1 CONCLUSIONS

This thesis confirms the applicability of rock typing from well logs in hydrocarbon-bearing shale formations. A synthetic case showed the benefit of inverted log properties over measured logs in the detection of rock types. The quality of well logs is negatively affected by shoulder-bed effects and averaging, especially in beds thinner than 2 ft. Inverted rock compositions are helpful for providing estimates of rock composition. However, the synthetic case showed that large errors can result from under-determined problems. Such under-determined problems are often encountered in practical applications. Furthermore, the assumptions included in a mineral model for inversion may be incorrect. Well logs and inverted properties are model independent (except for the placement of bed boundaries for inverted properties) and were reliable indicators of rock types in the field examples.

Core-data analysis is a necessary preliminary step to field applications of rock typing. Factor analysis was useful for reducing the plurality of well logs to avoid data overlap, and therefore, bias in the application of k-means cluster analysis. The highest-resolution well logs are recommended for the interpretation of thinly-bedded intervals. Neutron porosity, bulk density, and resistivity logs were used in a k-means cluster analysis. These conventional logs contain significant information which, when used jointly with k-means cluster analysis, can be used to estimate rock type distributions and to identify rock attributes.

A field case in the Barnett formation showed the possibility of thinly-bedded organic-rich layers. Rock typing performed on inverted log properties identified 40% more of the organic-rich rock type than rock types inferred from conventional well logs. The most important outcome in the lower Barnett formation example was the ability to distinguish a thinly-bedded organic-rich/organic-poor alternating sequence through rock typing where conventional estimates suggested less variability in kerogen concentration. Characterizing thin beds in shale gas reservoirs could result in more accurate integrated reservoir modeling when contrasted to the more homogeneous characterizations performed with conventional techniques.

A field case in the Haynesville formation showed a more uniform reservoir compared to the vertical variability observed in the Barnett formation. Only two rock types were identified from k-means cluster analysis. The study section in the Haynesville formation well belongs to a transitional slope-basin depositional environment. Rock types were interpreted to be a reflection of basin- or slope-trending depositional environments in the shale. This argument was supported by the average kerogen concentration, as determined from nonlinear inversion, of the respective rock types. Rock properties vary based on depositional environment due to composition; as a result, rock types can assist in determining additional reservoir characteristics based on formational/compositional associations.

The rock typing method developed here has potential applications for computing net-to-gross, performing well-to-well correlation, and improving reservoir modeling by determining rock type distributions.

6.2 SUGGESTIONS FOR FUTURE WORK

A necessity for successful shale gas projects is integration and optimization in a feedback loop cycle (Chong et al., 2010). Thorough geological verification would be appropriate to validate the rock types and production data would be necessary to confirm the highest-productivity zones. The effect of kerogen maturity on well logs and resultant rock classes would assist in identifying rock types which have generated the highest amount of hydrocarbon. A study on the effect of kerogen maturity on well logs would require large amounts of core data with which to definitively measure kerogen maturity.

Additionally, a larger-scale core study could also classify core-based rock types based on a variety of factors (mineralogy, organic content and maturity, pore size, saturation, etc.). Core-based rock types could be compared to well logs and well-log-based rock types. This approach could advance understanding of relationships between rock properties (measured in a laboratory) and well logs (measured in the wellbore) for the purpose of rock classification.

Mechanical properties have a significant impact on the fracture-stimulation potential and productivity of shale gas wells (Sondergeld et al., 2010). Considering the importance of mechanical properties, performing a supplementary analysis of mechanical properties and their relationship to fracture-prone shale would serve to enhance the value of rock typing for reservoir characterization.

Appendix A: Nonlinear Joint Inversion of Well Logs

Well-logging tools measure physical properties resulting from the unique combination of mineral and fluid constituents. Accurately estimating the volumetric concentration of rock components is crucial to shale gas formation evaluation. Mineral concentrations, fluid saturations, organic content, and porosity are indicators of the potential productivity of a reservoir. The spatial distribution of properties and compositions of organic shales vary significantly both vertically and laterally (Passey et al., 2010). The process of inversion in the algorithm used here treats shale as a sequence of stacked layers as described by Heidari et al. (2011). This method is referred to as a ‘nonlinear inversion’ because it does not assume linear relationships between mineral and fluid concentrations in the inversion process. It was found that neutron porosity and PEF well logs respond nonlinearly in the presence of complex mineralogy and gas. The model developed for the nonlinear inversion method also attempts to reduce shoulder-bed effects and reconcile differences between the volumes of investigation inherent to different measurement types.

A.1 MODEL DEVELOPMENT

A.1.1 Bed-Boundary Selection

The nonlinear inversion requires selection of bed boundaries to establish layers for a bed-by-bed estimation of properties as described in Chapter 2. The best results were achieved by manual selection of bed boundaries in the cases studied in this thesis.

A.1.2 Mineral Model

A review of quantitative mineral analysis from X-ray diffraction (XRD) was used to define the mineral model and benchmark inversion results. Figure A.1 shows the mineral model assumed in the nonlinear inversion.

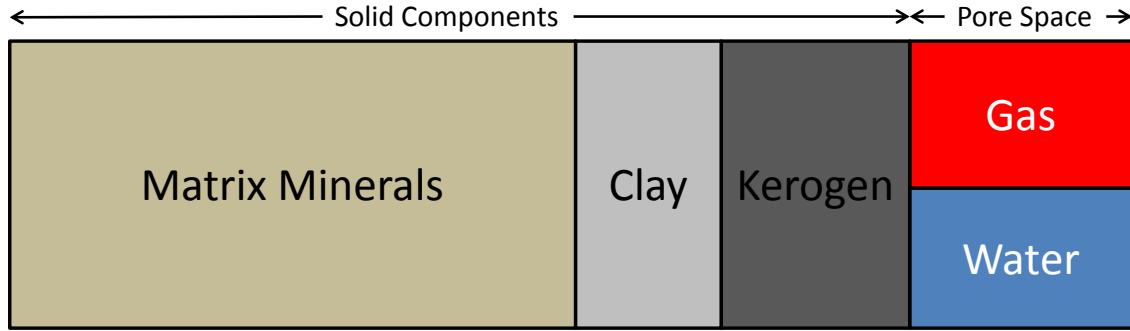


Figure A.1: Generalized mineral model assumed for volumetric calculations in Haynesville formation and Barnett formation shale gas plays.

A.2 INVERSION METHOD

Once bed boundaries are chosen to define layers, the inversion process estimates bed properties. The purpose of this initial inversion is to minimize shoulder-bed effects on well logs. Bed property estimation is performed by minimizing the quadratic cost function

$$C(\mathbf{p}) = \|\mathbf{d}(\mathbf{p}) - \mathbf{d}_m\|_2^2 + \alpha^2 \|\mathbf{p} - \mathbf{p}_o\|_2^2, \quad (\text{A.1})$$

where \mathbf{p} is a vector of layer-by-layer density, photo-electric factor (PEF), resistivity, or neutron porosity. The vector $\mathbf{d}(\mathbf{p})$ designates numerically simulated values for a particular property and \mathbf{d}_m is the corresponding vector of measurements (well logs). The factor α is a regularization (stabilization) parameter; \mathbf{p}_o is a vector that defines the reference model which can be chosen from either the average or center-bed values within

a layer. The gamma-ray, density, and PEF logs vary linearly with variations of layer properties. On the other hand, resistivity and neutron measurements vary nonlinearly with variation of layer properties in general. In the case of resistivity and neutron property inversion, the cost function from equation (A.1) is minimized using the Levenberg-Marquardt method with the numerical simulation for each respective well log performed to calculate the entries of the Jacobian matrix. Results from the first inversion produce estimates of layer-by-layer density, PEF, neutron migration length (Lm), true formation resistivity, and spectral gamma ray (thorium, uranium, and potassium). These estimated layer properties are used in a second, subsequent inversion to estimate the composition of shale for the model shown in Figure A.1. Schlumberger's SNUPAR software (McKeon and Scott, 1989) is used to calculate PEF and migration length for mineral compositions and concentrations in the inversion. Shale properties are estimated by minimizing the quadratic cost function

$$\mathcal{C}(\mathbf{x}) = \|\mathbf{W}_d \cdot (\mathbf{p}_i(\mathbf{x}) - \mathbf{p}_{mi})\|_2^2 + \alpha^2 \|\mathbf{x}\|_2^2, \quad (\text{A.2})$$

where \mathbf{x} is the vector of shale properties and mineral constituents, given by

$$\mathbf{x} = \begin{bmatrix} c_1 \\ c_2 \\ \vdots \\ c_i \\ c_{kerogen} \\ \phi_{total} \\ S_w \end{bmatrix}, \quad (\text{A.3})$$

where c_i designates the volumetric concentration of the i -th mineral constituent, \mathbf{W}_d is the data weighting matrix, $\mathbf{p}_i(\mathbf{x})$ is a vector of numerically simulated properties, and \mathbf{p}_{mi} is a vector that includes properties determined in the first inversion.

A.3 APPLICATION OF NONLINEAR INVERSION TO THE BARNETT FORMATION FIELD EXAMPLE

The nonlinear inversion described by Heidari et al. (2011) was performed on depth zones of interest in one well in the Barnett formation. Well logs used in the inversion were bulk density, neutron porosity, apparent array induction resistivity (deep), and photo-electric factor (PEF). Ideally, the highest resolution well logs should be used in the inversion to better resolve bed-level properties. Well logs that are the product of filtering, poorly performed processing, or adverse logging conditions are a significant source of error and uncertainty on inversion results. Gamma-ray logs were not used in the inversion because logging-site specific calibration constants were not available. Furthermore, gamma radiation properties for organic matter are highly variable and could not be accurately estimated.

Archie's equation (Archie, 1942) was used in the joint inversion to estimate porosity and saturation with the measured deep-reading apparent resistivity log. Archie's equation is given by

$$R_t = R_w \frac{a}{\phi^m} \frac{1}{S_w^n}, \quad (\text{A.4})$$

where R_t is true resistivity, R_w is resistivity of connate water, ϕ is total porosity, and S_w is total water saturation. The coefficient a is the tortuosity factor; m and n are the cementation and saturation exponents, respectively.

An equation has not been developed for applications in gas shales and the use of Archie's equation violates some of the assumptions made in its formulation (Torres-Verdín, 2010). Nevertheless, the lack of an appropriate model requires modification that should be—but is not—based on laboratory measurements. The exponents m and n were adjusted to match core data (ϕ, S_w) with field-measured apparent deep resistivity through equation (A.4). An initial rock classification was performed using cluster analysis in the study interval. Core points that fell in a rock class were assigned a grouping. This grouping would then form the basis for variable m and n exponents. Figure A.2 shows the result of matching core-calculated resistivities from Archie's equation (Archie, 1942) with variable m and n values to measured apparent resistivities. The m and n values obtained from this approach were then applied in the inversion to estimate *in situ* field saturations and porosity.

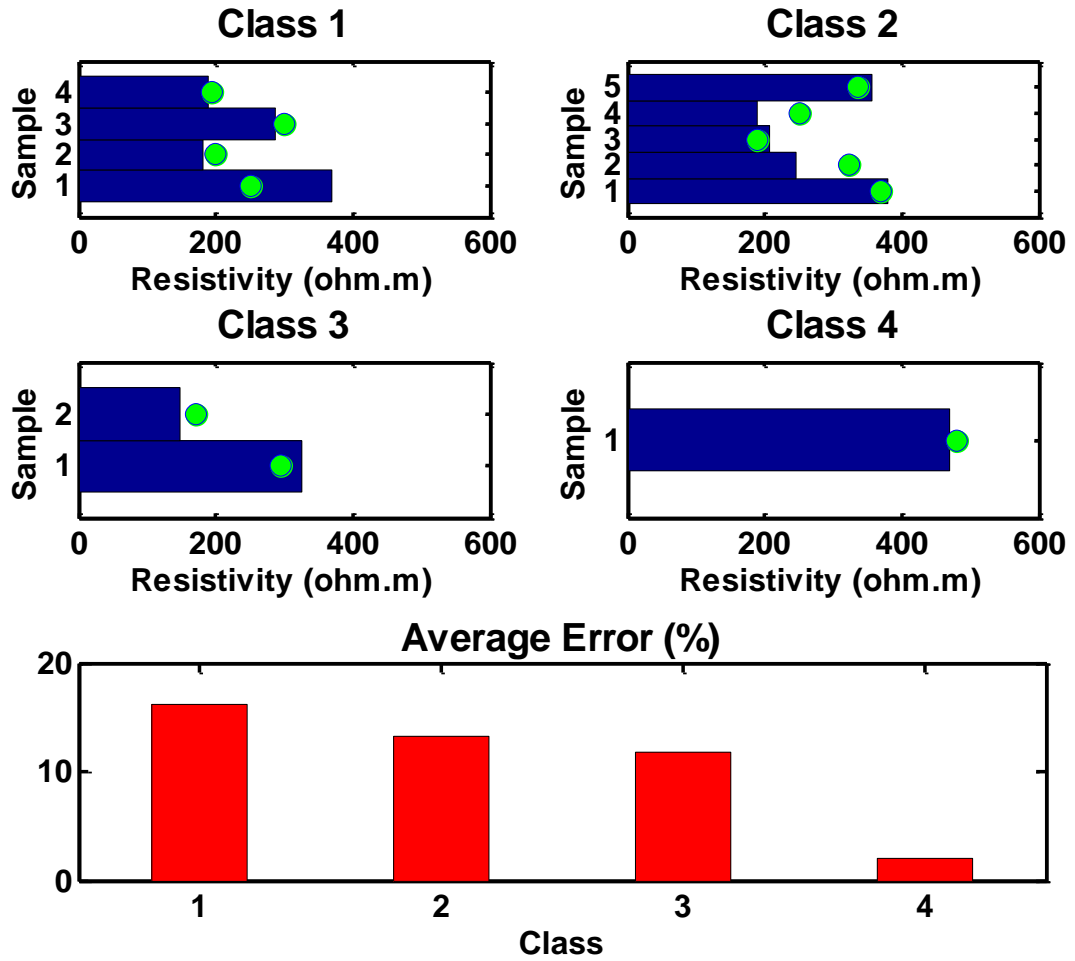


Figure A.2: Adjustment of resistivity exponents (a , m , n) by matching core saturation, porosity, and estimated connate-water resistivity to available resistivity measurements. For Class 1: $a=1$, $m=2.05$, $n=2$; for Class 2: $a=1$, $m=2.3$, $n=2$; for Class 3: $a=1$, $m=2.1$, $n=2$; for Class 4: $a=1$, $m=1.7$, $n=1.5$.

Figures A.3 to A.5 show results from the inversion performed in the lower Barnett formation. Figure A.3 shows the inverted-log layer properties as they compare to measured well logs. Figure A.4 shows the estimated mineral compositions (red, blocked) together with core data (blue circles). Figure A.5 shows the well logs simulated from the

inverted mineral estimates (red, dashed lines) as they compare to the original measured logs (blue, solid lines).

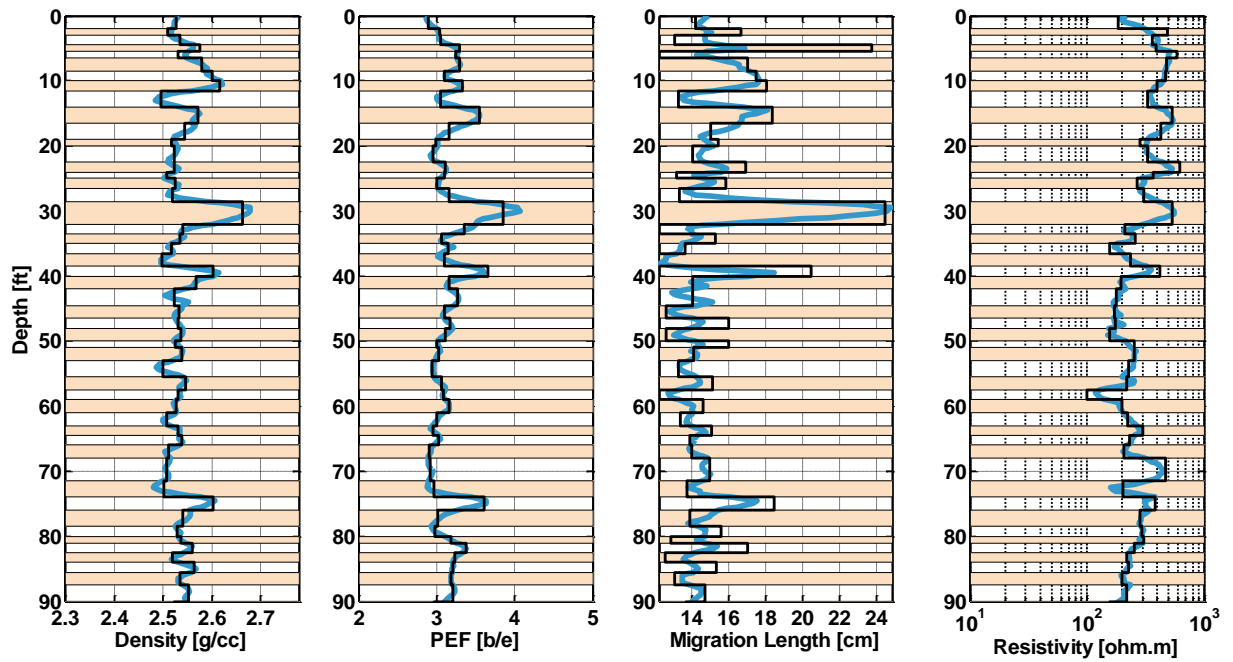


Figure A.3: Inverted layer properties compared to field measurements. Track 1: Measured and inverted density. Track 2: Measured and inverted PEF. Track 3: Measured and inverted migration length. Track 4: Measured and inverted deep resistivity.

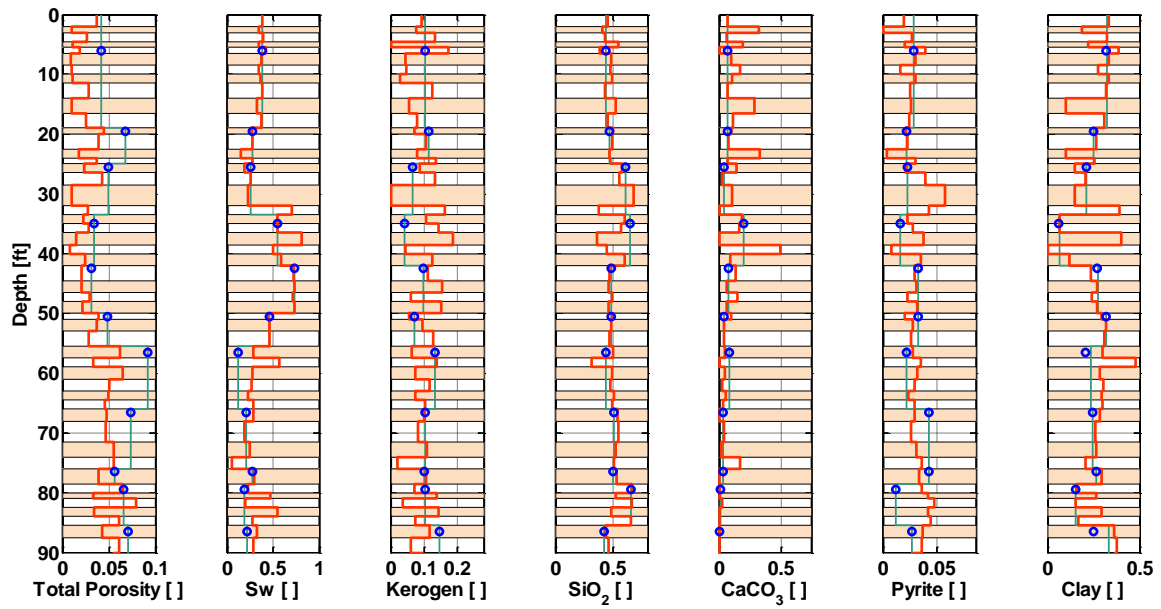


Figure A.4: Estimated shale composition from nonlinear inversion. Track 1: Total porosity. Track 2: Water saturation. Track 3: Volumetric concentration of kerogen. Track 4: Volumetric concentration of quartz. Track 5: Volumetric concentration of calcite. Track 6: Volumetric concentration of pyrite. Track 7: Volumetric concentration of clay.

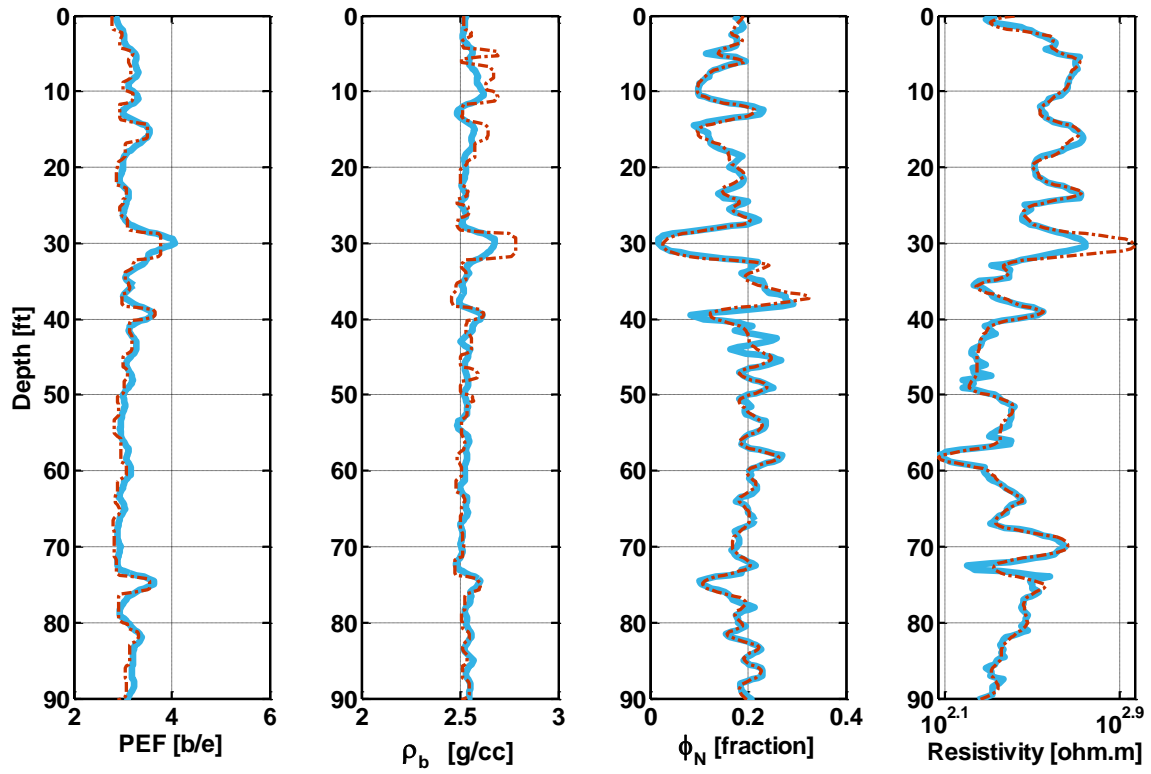


Figure A.5: Well logs numerically simulated from estimated rock components and their agreement with well logs. Track 1: Measured and simulated PEF. Track 2: Measured and simulated bulk density. Track 3: Measured and simulated neutron porosity (in limestone units). Track 4: Measured and simulated apparent deep resistivity.

Minerals	Chemical Formula	Density (g/cc)	Source
Quartz	SiO ₂	2.65	Zinsner and Pellerin (2007)
Calcite	CaCO ₃	2.71	
Pyrite	FeS ₂	5.01	
Illite	*	2.78	*Predefined in Schlumberger's SNUPAR code, McKeon and Scott (1989).
Kerogen	C _{6.5} H _{10.2} N _{0.12} S _{0.02} O _{0.32}	1.3	Yen and Chilingarian (1976)
Fluids			
Water	Salinity: 90,000 ppm NaCl equivalent		Zhao et al. (2007)
Gas	Density: 0.2 g/cc Chemical Formula: CH4		Estimated from Schlumberger Chartbook, Gen-8: Density and Hydrogen Index of Gas
Archie's Resistivity Parameters			
	<i>a</i>	<i>m</i>	<i>n</i>
Class 1	1	2.05	2
Class 2	1	2.3	2
Class 3	1	2.1	2
Class 4	1	1.7	1.5

Table A.1: Mineral, fluid, and resistivity values assumed in rock-compositional inversion for the lower Barnett formation well.

Appendix B: Calculation of TOC based on Passey's Method

Passey's method (Passey et al., 1990) is an empirical, well-log-based approach to estimate TOC. Well logs required for the estimation are resistivity in conjunction with a 'porosity' well log which can be one of the following: compressional sonic, neutron porosity, or density. In this thesis, the estimation was performed with both compressional sonic and apparent resistivity as well as bulk density and apparent resistivity. The remainder of this section shows the procedure used to estimate TOC concentration.

Density and resistivity logs were plotted on the same track and overlain in a non-organic rich interval. A value must be chosen in this interval to define the baseline for both curves. The corresponding TOC estimate is then calculated depth-by-depth with the following equation

$$\Delta \log R_{den} = \log_{10} \frac{R}{R_{baseline}} - 2.50 \times (\rho_b - \rho_{baseline}), \quad (B.1)$$

where $\Delta \log R_{den}$ quantifies the degree of separation between resistivity and density logs, R is apparent resistivity (ohm.m), $R_{baseline}$ is the baseline resistivity (ohm.m), ρ_b is bulk density (g/cc), and $\rho_{baseline}$ is the baseline bulk density (g/cc).

In order to calculate TOC, an estimation of the level of organic maturity, or LOM, must be made beforehand. Figure B.1 shows a plot of S2, which is a measure of the remaining hydrocarbon generative potential of kerogen, versus TOC (weight percent).

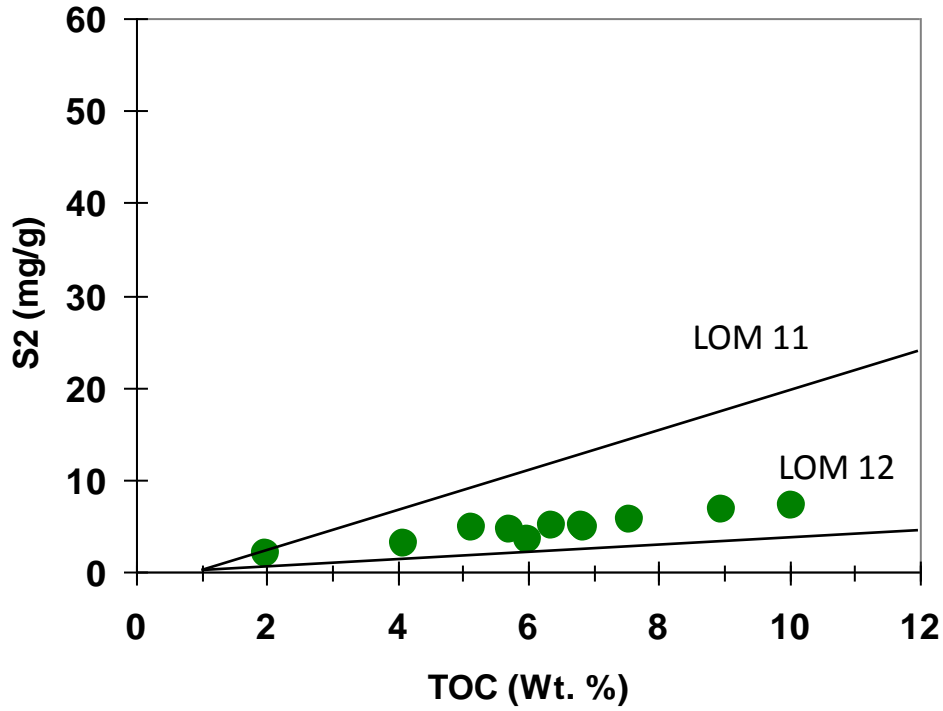


Figure B.1: Determination of LOM from a cross-plot of S2 vs. TOC obtained from laboratory measurements.

An LOM value of 11.8 was chosen from Figure B.1 based on overlay values (Passey et al., 1990). This LOM value is used in the calculation of TOC via the equation

$$TOC = \Delta \log R_{den} \times 10^{2.297 - 0.1688 \times LOM}, \quad (B.2)$$

where TOC is the calculated estimate of total organic carbon (wt. %), $\Delta \log R_{den}$ is calculated from equation (B.1), and LOM is the level of organic maturity estimated from Figure B.1.

Figure B.2 shows the input well logs (bulk density and apparent deep resistivity) and the outputs from the TOC estimation compared to core data. The last track compares

density-derived TOC and compressional-sonic-derived TOC to emphasize the similarity between results obtained with different input well logs.

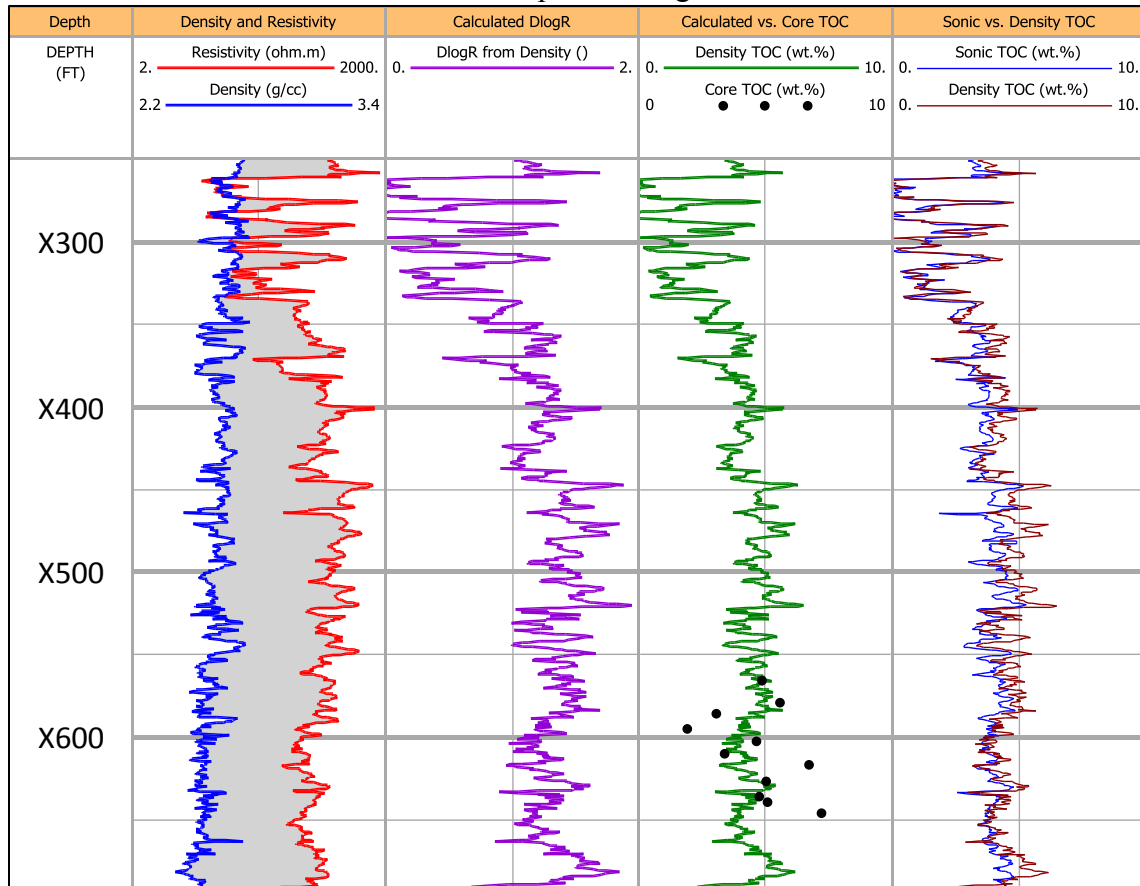


Figure B.2: Display of inputs and results from Passey's TOC-calculation method (Passey et al., 1990). Track 1: Relative depth. Track 2: Resistivity and density logs with grey shading indicating separation between the logs. Track 3: Delta log R calculated from the separation between density and resistivity. Track 4: TOC from Passey's method compared to core data. Track 5: Comparison between sonic/resistivity TOC calculation and density/resistivity TOC calculation.

Glossary

a	: Archie's tortuosity factor
AIT	Array Induction Tool, mark of Schlumberger
c_i	: Volumetric concentration of the i -th mineral constituent for nonlinear inversion
$\mathbf{d}(\mathbf{p})$: Numerically simulated values for layer properties for nonlinear inversion
\mathbf{d}_m	: Vector of field measurements for nonlinear inversion
FMI	: Formation Micro Imager
Lm	: Migration Length (cm)
LOM	: Level of Organic Maturity
m	: Archie's cementation exponent
n	: Archie's saturation exponent
NTG	: Net To Gross
\mathbf{p}	: Vector of layer properties for nonlinear inversion
$\mathbf{p}_i(\mathbf{x})$: Vector of simulated properties from nonlinear inversion
\mathbf{p}_{mi}	: Vector of properties determined in the initial nonlinear inversion
\mathbf{p}_o	: Vector of the reference model from nonlinear inversion
PEF	: Photoelectric Factor
ppm	: Parts per million
R	: Apparent deep resistivity (ohm.m)
$R_{baseline}$: Apparent deep resistivity baseline for Passey's method (ohm.m)
R_t or R_t	: True deep resistivity (ohm.m)
R_w	: Resistivity of connate water (ohm.m)
S2	: Remaining hydrocarbon generative potential (milligrams of hydrocarbon

	per gram of rock)
S_g	: Gas Saturation (% of pore space)
SNUPAR	: Schlumberger Nuclear Parameter Code
S_w or S_w	: Water saturation (% of pore space)
TOC	: Total Organic Carbon (wt. %)
\mathbf{W}_d	: Data weighting matrix for nonlinear inversion
\mathbf{x}	: Vector of shale properties for nonlinear inversion
XRD	: X-Ray Diffraction
α	: Regularization (stabilization) parameter for nonlinear inversion
$\Delta \log R_{den}$: Quantification of the degree of separation between bulk density and resistivity for Passey's method
ρ_b	: Bulk density (g/cc)
$\rho_{baseline}$: Baseline bulk density for Passey's method (g/cc)
ϕ_{total}	: Total porosity (%)

References

- Amaefule, J.O., Altunbay, M., Tiab, D., Kersey, D.G., and Keelan, D.K. "Enhanced Reservoir Description: Using Core and Log Data to Identify Hydraulic (Flow) Units and Predict Permeability in Uncored Intervals/Wells." *SPE 26436*. Houston, TX: Society of Petroleum Engineers, October, 1993. 205-220.
- Archie, G. E. "The Electrical Resistivity Log as an Aid in Determining Some Reservoir Characteristics." *Petroleum Technology*, 1942: 54 - 62.
- Buller, D., Hughes, S., Market, J., Petre, E., Spain, D., and Odumosu, T. "Petrophysical Evaluation for Enhancing Hydraulic Stimulation in Horizontal Wells." *SPE 132990*. Florence: Society of Petroleum Engineers, 2010.
- Chong, K.K., Grieser, B., Jaripatke, O., and Passman, A. "A Completions Roadmap to Shale-Play Development: A Review of Successful Approaches toward Shale-Play Stimulation in the Last Two Decades." *SPE 130369*. Beijing: Society of Petroleum Engineers, 2010.
- DeCoster, J. "Overview of Factor Analysis." August 1998. <http://www.stat-help.com/notes.html> (accessed July 2011).
- Gale, J.F.W., Reed, R.M., and Holder, J. "Natural Fractures in the Barnett Shale and their Importance for Hydraulic Fracture Treatments." *AAPG Bulletin*, V. 91, No. 4, 2007: 603-622.
- Hammes, U. "Methods for Correlating Mudrocks." *Class Lectures 5 and 6*. Austin, September 20, 2010.
- Heidari, Z., Torres-Verdín, C., and Preeg, W. E. "Improved Estimation of Mineral and Fluid Volumetric Concentrations in Thinly-Bedded and Invaded Formations." Perth: Society of Petrophysicists and Well Log Analysts, 2010.
- Heidari, Z., Torres-Verdín, C., and Preeg, W.E. "Quantitative Method for Estimating Total Organic Carbon and Porosity, and for Diagnosing Mineral Constituents from Well Logs in Shale-Gas Formations." Colorado Springs: The Society of Petrophysicists and Well Log Analysts, 2011.
- Johnston, J., Heinrich, P., Lovelace, J., McCulloh, R., and Zimmerman, R. "Stratigraphic Charts of Louisiana." *Louisiana Geological Survey Folio Series No. 8*. Louisiana Geological Survey, 2000.
- Kale, S., Rai, S.R., and Sondergeld, C.H. "Rock Typing in Gas Shales." *SPE 134539*. Florence, Italy: Society of Petroleum Engineers, September 2010.
- MacQueen, J. "Some methods for classification and analysis of multivariate observations." *Proceedings of the Fifth Berkeley Symposium on Mathematical*

- Statistics and Probability, Volume 1: Statistics*. Berkeley: University of California Press, 1967. 281-297.
- Papazis, P. K. "Petrographic Characterization of the Barnett Shale." *Master's Thesis*. The University of Texas at Austin, August 2005.
- Passey, Q.R., Bohacs, K.M., Esch, W.L., Klimentidis, R., and Sinha, S. "From Oil-Prone Source Rock to Gas-Producing Shale Reservoir - Geologic and Petrophysical Characterization of Unconventional Shale-Gas Reservoirs." *SPE 131350*. Beijing, China: Society of Petroleum Engineers, June 2010.
- Passey, Q.R., Creaney, S., Kulla, J.B., Moretti, F.J., and Stroud, J.D. "A Practical Model for Organic Richness from Porosity and Resistivity Logs." *AAPG, V. 74, No. 12*, 1990: 1777-1794.
- Perry, K., and Lee, J. "Topic Paper #29: Unconventional Gas." National Petroleum Council, July 2007.
- Pittman, E. D. "Relationship of Porosity and Permeability to Various Parameters Derived from Mercury Injection-Capillary Pressure Curves for Sandstone." *AAPG Bulletin, V. 76, No. 2* (February 1992): 191-198.
- Rickman, R., Mullen, M., Petre, E., Grieser, B., and Kundert, D. "A Practical Use of Shale Gas Petrophysics for Stimulation Design Optimization: All Shale Plays Are Not Clones of the Barnett Shale." *SPE 115258*. Denver: Society of Petroleum Engineers, 2008.
- Schlumberger. "Log Interpretation Charts." Sugar Land, 2009.
- Sondergeld, C.H., Newsham, K.E., Comisky, J.T., Rice, M.C., and Rai, C.S. "Petrophysical Considerations in Evaluating and Producing Shale Gas Resources." *SPE 131768*. Pittsburgh: Society of Petroleum Engineers, 2010.
- Spears, R. W. and Jackson, S. L. "Development of a Predictive Tool for Estimating Well Performance in Horizontal Shale Gas Wells in the Barnett Shale, North Texas, USA." *Petrophysics, V. 50, No. 1*, 2009: 19-31.
- Torres-Verdín, C. *Integrated Geological-Petrophysical Interpretation of Well Logs*. Austin, 2010.
- Vernik, L. and Milovac, J. "Rock Physics of Organic Shales." *The Leading Edge*, 2011: 318-322.
- Xue, D., Rabinovich, M., Besspalov, A., and Corley, B. "Characterization of Fracture Length and Formation Resistivity from Array Induction Data." Austin, Texas: Society of Petrophysicists and Well Log Analysts, 2008.
- Yen, T.F. and Chilingarian, G.V. *Oil Shale*. Amsterdam: Elsevier, 1976.

- Zhao, H., Givens, N.B., and Curtis, B. "Thermal Maturity of the Barnett Shale determined from Well-Log Analysis." *AAPG Bulletin*, V. 91, No. 4, 2007: 535-549.
- Zinszner, B. and Pellerin, F. *A Geoscientist's Guide to Petrophysics*. Paris: Editions Technip, 2007.